Total water level prediction at continental scale: coastal ocean

Linlin Cui[a], Fei Ye[a], Y. Joseph Zhang[a*], Haocheng Yu[a], Zhengui Wang[a], Saeed Moghimi[b], Gregory Seroka[b], Jack Riley[b], Shachak Pe'eri[c], Soroosh Mani[b,d], Edward Myers[b], Kyungmin Park[e], Liujuan Tang[b], Zizang Yang [b], Yan-Ming Wang[c]
[a] Virginia Institute of Marine Science, William & Mary, Gloucester Point, VA 23062, USA
[b] Coast Survey Development Laboratory, NOAA, Silver Spring, MD 20910, USA
[c] National Geodetic Survey, NOAA, Silver Spring, MD 20910, USA
[d] Spatial Front Inc., Bethesda, MD, 20817, USA
[e] Pacific Northwest National Lab, Seattle, WA 98109, USA

*Corresponds to: Joseph Zhang (yjzhang@vims.edu)
Submitted to: Ocean Modelling Special Issue "In silico oceanography via seamless cross-scale modeling: Are we there yet?"

Abstract

We demonstrate recent progress made in the simulation of total water level (TWL) at continental scale, using the coastal ocean of US East Coast/Gulf of Mexico coast as an example. A key difference between the continental-scale and small-scale modeling is that the former requires a more accurate vertical datum. Using a geoid-based datum (xGEOID20b), a satellite altimetry product, and a state-of-the-art 3D unstructured-grid model, we significantly improve the accuracy for TWL both near- and off-shore. The average root-mean-square error at all NOAA stations is 14 cm. The non-tidal signals are found to be sensitive to the representation of a large-scale current system near the boundary and extending the domain extent to accommodate this system improves these signals.

Key words: total water level; geoid; cross-scale modeling; continental scale; thermohaline steric effects; SCHISM

1. Introduction

Accurate prediction of the total water level (TWL) is of paramount importance for coastal disaster planning and mitigation to achieve community resilience (Stockdon et al., 2023). TWL in this paper is defined as the observed water level at a place, and thus includes all physical forcings (tides, waves, atmosphere, rivers, groundwater, and precipitation etc). Recent advances in full coupling of hydrologic models into the coastal models (Ye et al., 2020; Huang et al. 2021; Stephens et al., 2022) pave the way for better TWL prediction. Previously we have demonstrated the potential of a 3D modeling approach that simultaneously includes all those forcings as required by TWL prediction in a single unstructured-grid model (Huang et al., 2021). In this paper, we will present the results applying this approach to a continental scale problem. We will however neglect the contributions from wind waves and groundwater to TWL here, as these effects are arguably small during non-storm period. We have previously demonstrated the wave effects in Hurricane Florence (Ye et al., 2021).

Unlike regional modeling, continental-scale modeling is much more challenging as it must integrate across processes of disparate scales. In return, a great benefit of continental-scale modeling is that it can be easily used to investigate the nonlinear interactions among large- and small-scale processes. Ezer (2018) and Ye et al. (2020) are among the first to demonstrate the

importance of such interactions as they investigated the impact of the Gulf Stream oscillation on coastal water levels. In fact, most of the non-tidal water level variability at the continental scale can be attributed to large-scale processes. As far as modeling is concerned, there are two main challenges. First, an accurate vertical datum needs to be defined, preferably a non-tidal datum to avoid the changes in tidal epochs and sea-level rise. For example, Jahanmard et al. (2021) applied a geoid-based datum for the Baltic Sea and obtained promising results. Second, unless a global ocean model is used, the open boundary condition needs to be sufficiently accurate, with respect to the vertical datum. Most large-scale models use mean sea level as the datum and have biases in the open ocean, even if data assimilation is applied.

In this and other related papers, we demonstrate progress made and various remaining issues related to the simulation of TWL at continental scale, using two examples from the US East Coast/Gulf of Mexico coast and Great Lakes. We focus on the coastal ocean of east Coast/Gulf of Mexico coast in this paper. Specifically, we utilize a geoid-based datum, xGEOID20b, which was recently developed by NOAA to facilitate continental-scale modeling (Wang et al., 2022). The xGEOIDs provide a sneak preview of the changes expected from the upcoming North American-Pacific Geopotential Datum of 2022 (NAPGD2022). In addition, a satellite altimetry product, AVISO's absolute dynamic topography (ADT; http://www.aviso.altimetry.fr/; last accessed in March 2024), which provides estimate of the gridded sea level above geoid, is used to drive the model at the ocean boundary (as the non-tidal component) and to provide the initial condition of sea surface. We combine this information with a state-of-the-art 3D unstructured-grid model to significantly improve the accuracy for TWL both near- and off-shore.

In Section 2, we describe the observation datasets used to validate the model, the new vertical datum adopted, and the model setup. Section 3 presents model validation for tidal, non-tidal, and TWL and surface currents. In Section 4, we discuss a few important issues in the continental-scale modeling, using sensitivity tests to demonstrate the importance of 3D thermohaline steric effects and the remote effect from Gulf of St. Lawrence on Gulf of Maine. Section 5 summarizes this work.

2. Methods

2.1 Observation

A comprehensive analysis is carried out to assess the model's ability to capture the TWL along the US East Coast and Gulf of Mexico coast. Since we have previously assessed the model skill for temperature and salinity at large scales (Ye et al. 2020; Huang et al. 2021), we will focus on elevation and currents in this paper. The observational data used include all tide gauges maintained by NOAA CO-OPS (https://tidesandcurrents.noaa.gov/map/index.html; last accessed in March 2024), with a total of 164 stations included. Most gauges provide observation data with respect to NAVD88. The simulation period of year 2015 is selected to maximize the data availability. An important data source used to both initialize and assess the model skill is AVISO global ADT products (https://data.marine.copernicus.eu/product/SEALEVEL_GLO_PHY_L4_MY_008_047/services; last accessed in March 2024). Note that tides have been removed from ADT, so the latter represents the non-tidal component of TWL in the ocean. The model's skill for the surface currents is assessed against CODAR (Coastal Ocean Dynamics Application Radar) SeaSonde HF radar system (https://cordc.ucsd.edu/projects/hfrnet/; last accessed in March 2024). The

measured surface velocities are representative of the upper 0.3-2.5 m of the ocean. CODAR can measure currents up to 200 km from the coast with a spatial resolution of 1-6 km depending on the radar frequency. In this study, hourly, 6-km current data were obtained from the National Centers for Environmental Information (NCEI, s://www.ncei.noaa.gov/data/oceans/ndbc/hfradar/rtv; last accessed in March 2024) to validate the model's performance on surface currents. As will be discussed later, the thermohaline steric effects are the main driver of the non-tidal component of TWL, so it's important for the model to be able to correctly capture the current systems in this domain.

2.2 Vertical datums

In all hydrodynamic studies, both surface water level and bottom elevation (bathymetry) must be measured against a reference datum ("zero height"). Historically, both geoid (aka geopotential; Pugh 1987) and non-geoid based datums have been used. One of the first vertical datums proposed for the US waters is Sea Level Datum of 1929 (SLD 29), which set the "zero height" at 26 tide gauges, including five in Canada. Since the mean sea level differed from location to location, SLD 29 was later renamed as National Geodetic Vertical Datum of 1929 (NGVD 29) to account for the geodetic aspect of the datum. NGVD 29 was the official U.S. vertical datum until it was replaced by North American Vertical Datum of 1988 (NAVD 88) in 1991 (Zilkoski et al. 1992). NAVD 88 contained more data of leveling and was calculated using strict mathematical models. It somewhat rectified the distortions in NGVD 29 and thus improved the elevation accuracy. However, NAVD 88 is referenced to a single tidal gauge in Quebec, Canada, which opened the possibility of unconstrained cross-continent error build-up.

Theoretically, the ideal vertical datum for large-scale simulations is a geoid, which is the equipotential surface that would be assumed by the sea surface in the absence of tides, water density variations, currents and atmospheric effects (Pugh 1987). It varies above and below the geometric ellipsoid of revolution by as much as 100 m due to the uneven distribution of mass within the Earth. Through more accurate geophysical modeling, NOAA is close to finishing the development of the next-generation geoid reference (https://geodesy.noaa.gov/library/pdfs/NOAA_TR_NOS_NGS_0064.pdf; last accessed in March 2024), and the latest version publicly available at the time of this study, xGEOID20b, will be used as the vertical reference datum in this paper (Wang et al., 2022). This geoid model uses the current static epoch of 2020.0 (https://beta.ngs.noaa.gov/GEOID/xGEOID20/index.shtml).

When necessary, both model and observation are converted into xGEOID20b for direct comparison, using NOAA's VDatum tool ((https://vdatum.noaa.gov/; last accessed in March 2024). Therefore, the errors and uncertainties in the current model setup come from multiple sources due to: (1) the VDatum conversion among datums; (2) difference between AVISO/ADT's geoid (GOCO06S; Kvas et al, 2021) and xGEOID20b, which is not accounted for in the model; (3) large vertical land motion (https://www.sonel.org/-Vertical-land-movements-.html) in some areas like the Gulf Coast, where geoid models tend to have larger uncertainties. These errors and uncertainties explain the need for adjusting the ADT derived boundary condition at our ocean boundary (see Section 2.3). We will revisit this issue after the official geoid is finalized. We also noted that the estimated uncertainties associated with VDatum and ADT are relatively small, no more than 10 cm from each source

(https://drive.google.com/file/d/1nRr5HKfC0G1AFVH3gIemfICPgiNTL0gW/view?usp=drive_link; https://www.aviso.altimetry.fr/en/data/products/auxiliary-products/mdt/mdt-global-cnes-cls/description.html).

2.3 Model configuration

We use the open-source SCHISM hydrodynamic model (schism.wiki, last accessed in March 2024), which solves the hydrostatic, Boussinesq, primitive equations on a hybrid triangular-quadrangular unstructured grid in the horizontal dimension and hybrid Localized Sigma Coordinates with Shaved Cells (LSC^2) grid in the vertical dimension (Zhang et al., 2015, 2016). The model is grounded on accurate, robust and efficient semi-implicit time stepping scheme (with no mode splitting) and a hybrid finite-element/finite-volume formulation. The numerical dissipation is kept low with a few higher-order, monotone schemes (Ye et al. 2019).

The model domain is largely based on Fei et al. (2023), and is intended to be the upgraded version of NOAA's 3-D Surge and Tide Operational Forecast System for the Atlantic Basin (https://registry.opendata.aws/noaa-nos-stofs3d/, hereafter referred to as STOFS3D-v4). The upgraded STOFS3D (hereafter referred to as STOFS3D-v6) includes Gulf of St. Lawrence (Fig. 1). The domain covers the US East Coast and Gulf of Mexico coast, with the land boundary located at 10 m above mean sea level to incorporate NWM (National Water Model) river flows there (Zhang, 2020). In addition, all major bays, estuaries, and coastal watersheds are well resolved to facilitate the study of compound flooding. The horizontal grid has 2.93 million nodes and 5.65 million elements. The horizontal grid resolution varies from 6-7 km along the ocean open boundary to ~500 m near the coastline. In the coastal watersheds, rivers and creeks have a resolution of about 300 m along-channel and variable resolutions cross-channel to ensure that channels are resolved regardless of their widths. The watershed portion of the mesh is automatically generated using the algorithm described in Ye et al. (2023). This approach is an upgrade from the 1D NWM river network approach used in v4 (Huang et al., 2021; Ye et al., 2021). Most defense features like levees are resolved with a high resolution as fine as 1 m based on the National Levee Database (https://levees.sec.usace.army.mil/#/; last accessed in March 2024).

A combination of different digital elevation model (DEM) sources is used for mesh generation and mesh bathymetry, including GEBCO (https://www.gebco.net/; last accessed in March 2024), CRM (https://www.ncei.noaa.gov/products/coastal-relief-model; last accessed in March 2024) CUDEM (https://www.ncei.noaa.gov/metadata/geoportal/rest/metadata/item/gov.noaa.ngdc.mgg.dem:999919/html; last accessed in March 2024) and CoNED (https://topotools.cr.usgs.gov/topobathy_viewer/; last accessed in March 2024) (cf. Ye et al., 2023). CUDEM and CoNED assume the NAVD 88 datum, while other DEMs assume local MSL. The bathymetry information in the DEMs is linearly interpolated onto the mesh; in the overlapping areas with multiple DEMs available, only the DEM of highest quality is used in interpolation (e.g., CUDEM is preferred over GEBCO). The mesh bathymetry near coast is then converted to xGEOID20b using the VDatum software; no datum adjustment is done at the nodes that fall outside VDatum's coverage (Fig. 1) or if the DEM is not on NAVD88 (fortunately, these cases correspond to deeper depths so the errors committed by not converting the datums would only marginally affect the model accuracy). After this conversion, no further manipulation of

bathymetry (e.g., bathymetry smoothing) is done, which represents a major difference between SCHISM and other coastal models and has important implications on model's representation of coastal processes (Zhang et al. 2024).

The atmospheric forcing data are obtained from European Centre for Medium-Range Weather Forecasts (ECMWF) atmospheric reanalysis product ERA5 (https://www.ecmwf.int/en/forecasts/dataset/ecmwf-reanalysis-v5; last accessed in March 2024), which has a horizontal resolution of ~31 km. Near the coast, NOAA's High-Resolution Rapid Refresh (HRRR; https://rapidrefresh.noaa.gov/hrrr/; last accessed in March 2024) is used, with 3km and hourly resolution. The atmospheric analysis variables used by SCHISM are air temperature at 2 m, wind velocity at 10 m, mean-sea-level pressure, specific humidity, precipitation rate, and surface downward long-wave and short-wave radiation fluxes. The air-sea fluxes for momentum and heat are calculated according to the bulk aerodynamic formulation of Zeng et al. (1998). The watershed inflow is derived from the NWM retrospective dataset (https://registry.opendata.aws/nwm-archive/; last accessed in March 2024) and is injected at the 1238 intersecting locations between NWM network and our land boundary. Unlike the previous v4 setup (Huang et al., 2021), the source locations may be relocated to the nearest NWM rivers due to some mismatches between the NWM network and new channel thalwegs that are automatically calculated from the raw DEMs. Since the domain is expanded to include Gulf of St. Lawrence, the St. Lawrence River, a large river with an annual mean discharge of over 14,000 m^3/s, is also added into the model. We use the same flow data for this river as Wang et al. (2022b), which was estimated based on a correlation with an upstream station. The river temperature for this river is interpolated from the satellite GHRSST product (GHRSST Project Office et al., 2023).

The initial and (non-tidal component of) boundary conditions are derived from AVISO (ADT) for the elevation, and HYCOM for velocity, salinity and temperature. Since none of these sources include tides, the FES2014 tidal database is used to add tidal elevation and (barotropic) velocity at the ocean boundary (with 8 major tidal constituents). Assessment of the HYCOM temperature against satellite and ARGO float observation data revealed that HYCOM temperature is on average 1.8 ℃ lower than the observation in our model domain. Therefore, to better simulate the Gulf Stream, we apply a simple bias correction of +1℃ uniformly across the water column to the HYCOM water temperature. This method keeps the temperature gradient unchanged. In addition, salinity and temperature are relaxed to the HYCOM values near the open boundary (within 7.3° from the open ocean boundary), with the maximum relaxation scale of 1 day. Like Lopez et al. (2020), a vertical datum offset is applied to ADT for both initial and boundary conditions, which may be attributed to the uncertainties mentioned above. Sensitivity tests for the coastal water levels at the 164 NOAA tide gauges suggest a uniform adjustment of -0.42 m is sufficient for our purpose. Further tuning of this offset was done after this paper during the NOAA operational forecast deployment, and -0.32 m was found to give even better results.

The simulation is initialized on December 1, 2014, at 00:00 UTC, and covers 396 days, with a time step of 150 s. The vertical mixing is parameterized using the generic length-scale model of *k-kl* (Umlauf and Burchard, 2003). The transport scheme for tracers is the 3rd order WENO (Ye et al., 2019) with a cutoff depth of 5 m, with a more efficient upwind scheme being used in depths shallower than 5m. The smoothness parameter in WENO, which controls the numerical

dispersion, is set to 10^{-6}. A Smagorinsky-like filter is applied to control the numerical dissipation/viscosity (Zhang et al. 2023). The first month was discarded as the warm-up period; we focus on the analysis of 2015 results in this paper.

The 3D model described above includes all forcings as required for the TWL prediction except the wave and groundwater effects and steric effects due to thermal expansion. While SCHISM has an internal spectral wave model and a coupled wave-current model has been applied before (Ye et al., 2021), we neglect the wave effects in this paper as our primary focus is on the long-term time series and wave effects are generally small during non-storm periods. We will leave it to future work to quantify this and other errors.

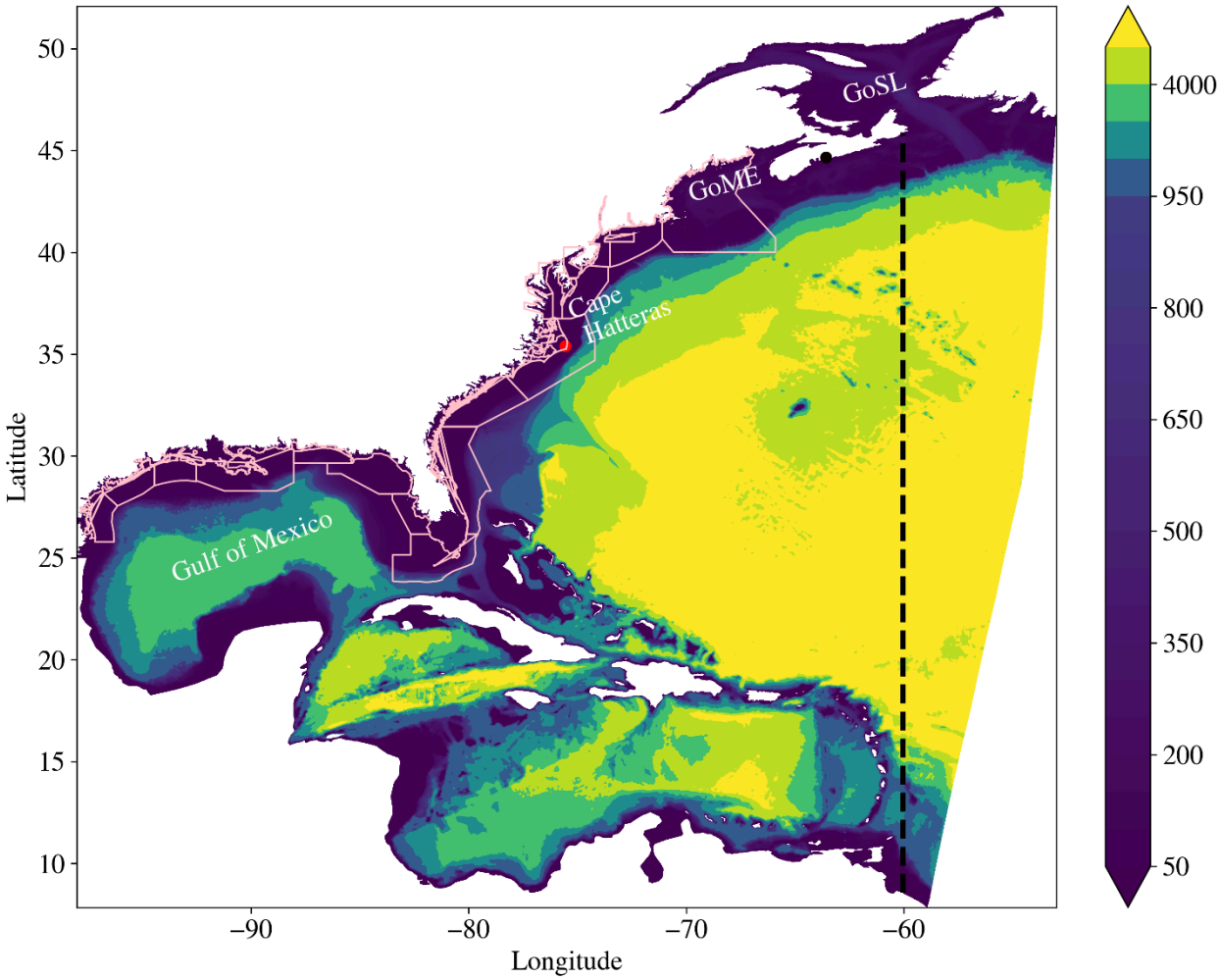

Fig. 1. STOFS3D-v6 domain including Gulf of St. Lawrence (the dotted line representing STOFS3D-v4 boundary). The color represents bathymetry in meters. Pink polygons show VDatum coverages. Some geographic features are also shown: GoME – Gulf of Maine, GoSL – Gulf of St. Lawrence; Gulf of Mexico; Cape Hatteras.

3. Model validation

In this section, the model performance is assessed for the tides and TWL against NOAA CO-OPS tide gauges in both coastal and inland areas. Long-term averaged sea surface height is compared against satellite altimetry. The simulated surface currents are assessed against CODAR. The model analysis interval is from January 1 to December 31, 2015.

3.1 Tidal elevation

Most of the stations along the east coast are dominated by the semi-diurnal M2 constituent, while diurnal K1 is the dominant frequency for many stations along the Gulf of Mexico. Fig. 2 and Fig. 3 show the amplitudes and phases of M2 and K1 at stations along the US East Coast (ordered from north to south) and Gulf of Mexico (ordered from east to west), respectively. For clarity, all inland stations with observed M2 amplitude less than 10 cm *and* K1 amplitude less than 5 cm are excluded in the comparison. This results in 49 stations for the US East Coast and 47 stations for Gulf of Mexico (Tables 1 and 2). For the east coast, the M2 amplitude at over two thirds of stations exceeds 0.5 m, with the largest amplitude of ~1 m at Gulf of Maine stations (the first 7 stations in Fig. 2). The M2 amplitude at the stations sheltered behind barrier islands is generally less than 0.2 m: for example, station 8652587 and station 8654467 in Fig 2a. The K1 amplitude at the US East Coast stations is much smaller than M2, around 0.1 m (Fig. 2c). The stations in the southeastern Gulf coast are still dominated by semi-diurnal tide (M2) (first nine stations in Fig. 3a), while other areas of Gulf coast, including the Mississippi Delta and Texas-Louisiana coast are dominated by the diurnal tide K1, with the amplitude generally less than 0.2 m. The model captures the large variability of tides in this domain (Figs. 2, 3). The linear regression between the observed and modeled amplitudes and phases confirms good model performance (Fig. 4), especially for M2. The outliers of K1 amplitude are mainly from four stations in 8737138, 8738043, 8760721, 8767816 (Fig. 3c and 4b). The total error for a single tidal constituent at a station can be assessed using the complex Root-Mean-Square Error (RMSE) that includes both amplitude and phase errors (Wang et al., 2012; Huang et al. 2022);:

$$RMSE = (0.5\times((A_o cosP_o - A_m cosP_m)^2 + (A_o sinP_o - A_m sinP_m)^2))^{1/2} \quad (1)$$

where A is the amplitude, P is the phase, "o" and "m" refer to observation and model. The average complex RMSE for M2 over all stations is 5.6 cm for v6, which is 0.9 cm smaller than 6.5 cm for v4. The total tidal error can be assessed using the total complex RMSE from 8 major constituents (M2, S2, N2, K2, K1, O1, P1, Q1), and is 6.6 cm for v6 (vs. 7.0 cm for v4). Fig. 5 shows the spatial distribution of complex RMSE for M2. Unsurprisingly, large errors are in the meso- and macro-tidal regions and at some inland stations.

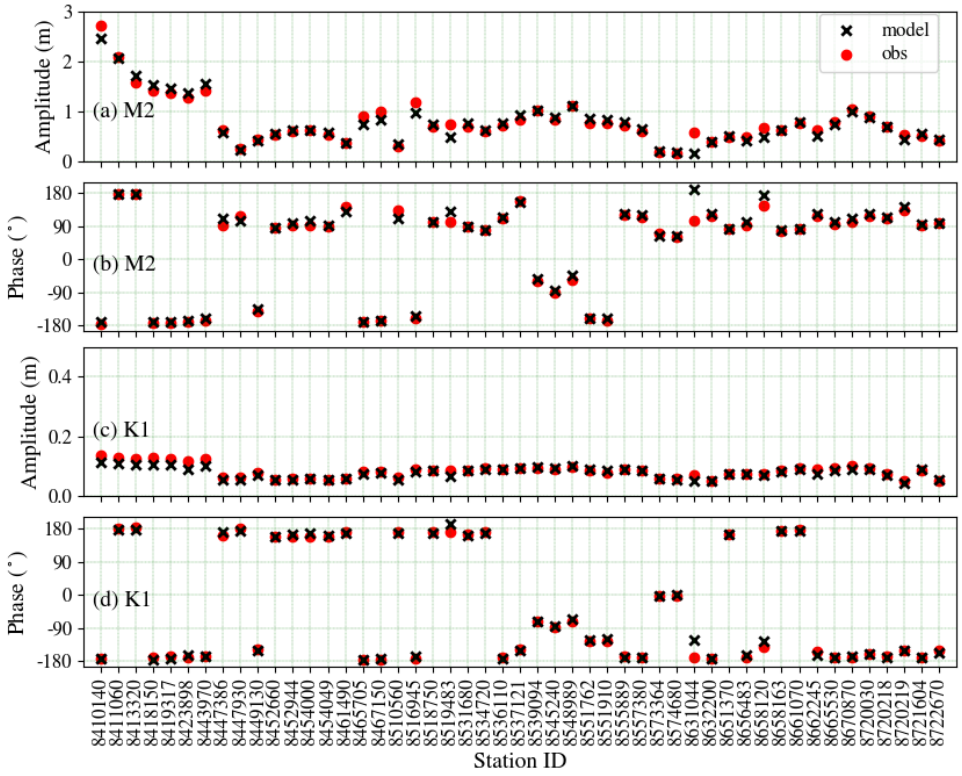

Fig. 2: Comparison of the harmonics between observation and model results for the NOAA CO-OPS stations along the U.S. East Coast (stations ordered from north to south). (a) Amplitude of M2, (b) phase of M2, (c) amplitude of K1, and (d) phase of K1.

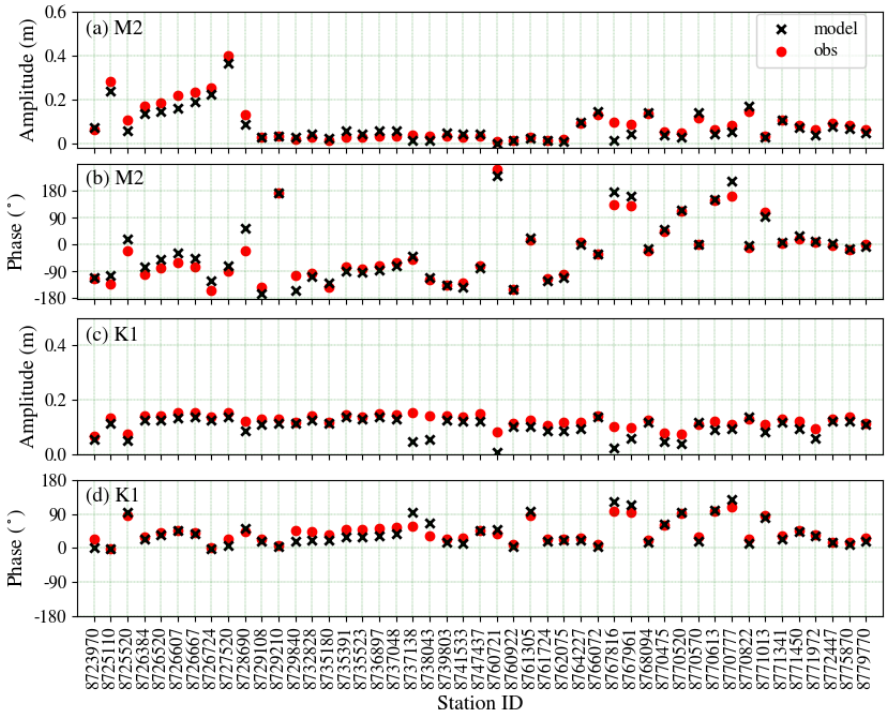

Fig. 3: Same as Fig. 2 but for the NOAA CO-OPS stations along the Gulf of Mexico coast (stations ordered from east to west).

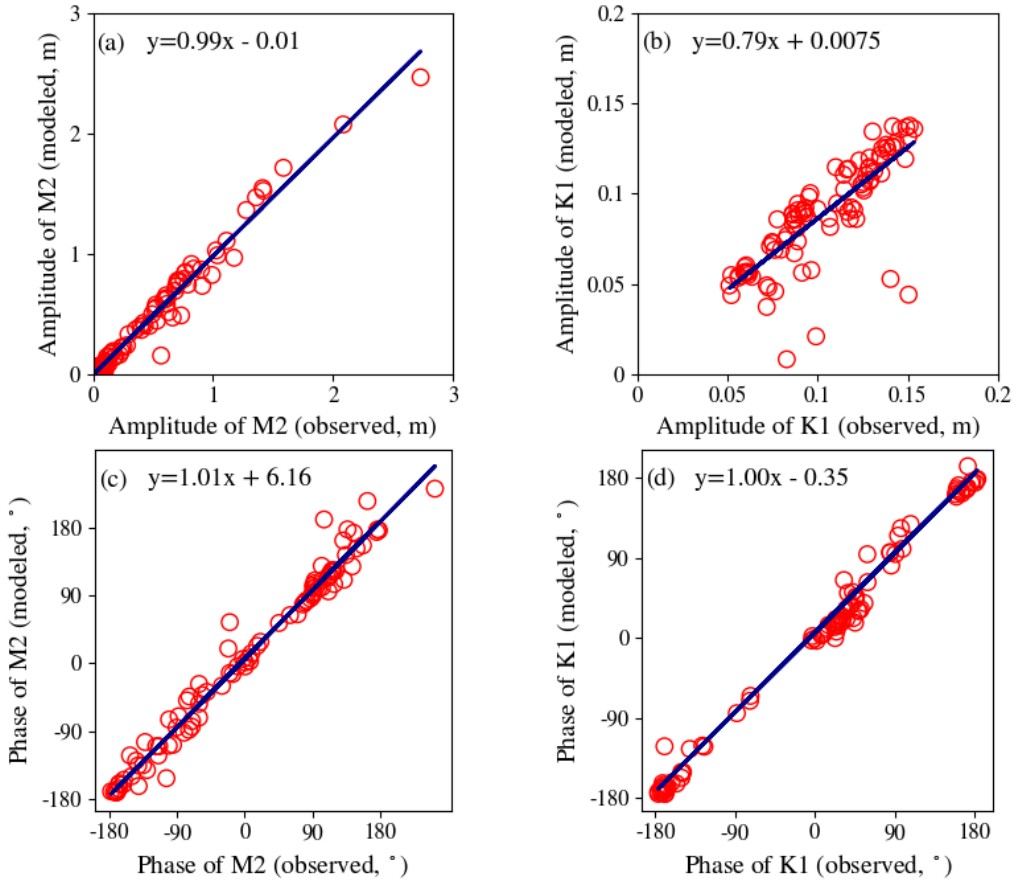

Fig. 4: Model-data comparison of the harmonic amplitudes and phases. The equations inside each panel are from the linear regression and the solid lines represent the perfect fit. (a) amplitude of M2, (b) amplitude of K1, (c) phase of M2, and (d) phase of K1.

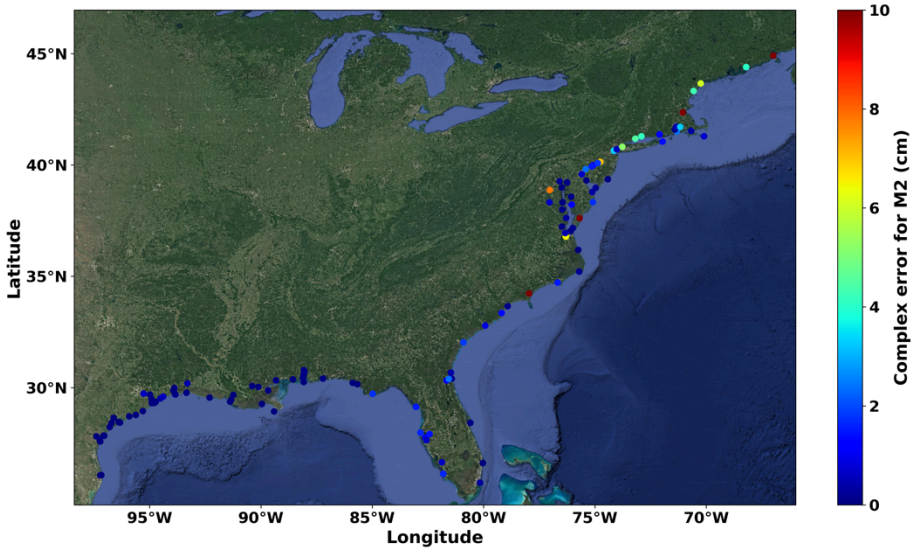

Fig. 5: Spatial distribution of complex M2 errors at the NOAA stations from STOFS3D-v6.

Table 1: Information of NOAA CO-OPS stations on US east coast

Station ID	Station Name	Longitude	Latitude
8410140	Eastport	-66.98290	44.90459
8411060	Cutler Farris Wharf	-67.20466	44.65702
8413320	Bar Harbor	-68.20427	44.39219
8418150	Portland	-70.24417	43.65806
8419317	Wells	-70.5633	43.32
8423898	Fort Point	-70.710556	43.07138
8443970	Boston	-71.05028	42.3539
8447386	Fall River	-71.164101	41.7043
8447930	Woods Hole	-70.671112	41.52361
8449130	Nantucket Island	-70.09639	41.28527
8452660	Newport	-71.326139	41.50433
8452944	Conimicut Light	-71.345167	41.71711
8454000	Providence	-71.400667	41.80716
8454049	Quonset Point	-71.41	41.58694
8461490	New London Thames River	-72.095556	41.37166
8465705	New Haven	-72.908333	41.28333
8467150	Bridgeport	-73.183969	41.17581
8510560	Montauk	-71.959444	41.04833
8516945	Kings Point	-73.765711	40.81134
8518750	The Battery	-74.014167	40.70055
8519483	Bergen Point West Reach	-74.146306	40.6391
8531680	Sandy Hook	-74.009389	40.46683
8534720	Atlantic City	-74.418053	39.35666
8536110	Cape May	-74.959999	38.9683
8537121	Ship John Shoal	-75.376678	39.30538
8539094	Burlington Delaware River	-74.869698	40.08169
8545240	Philadelphia	-75.141981	39.93305
8548989	Newbold	-74.751833	40.13733
8551762	Delaware City	-75.588972	39.58219
8551910	Reedy Point	-75.571944	39.55833
8555889	Brandywine Shoal Light	-75.113	38.987
8557380	Lewes	-75.119278	38.78283
8573364	Tolchester Beach	-76.244556	39.21344
8574680	Baltimore Patapsco River	-76.579444	39.26694
8631044	Wachapreague	-75.685833	37.60777
8632200	Kiptopeke	-75.988444	37.16519
8651370	Duck	-75.746696	36.1833
8656483	Beaufort Duke Marine Lab	-76.670658	34.71733
8658120	Wilmington	-77.953611	34.2275

8658163	Wrightsville Beach	-77.786667	34.21333
8661070	Springmaid Pier	-78.916389	33.65555
8662245	Oyster Landing N Inlet Estuary	-79.1867	33.3517
8665530	Cooper River, SC	-79.923611	32.78083
8670870	Fort Pulaski	-80.903028	32.03469
8720030	Fernandina Beach	-81.465842	30.67135
8720218	Mayport Bar Pilots Dock	-81.427889	30.39816
8720219	Dames Point	-81.559166	30.38722
8721604	Trident Pier	-80.593056	28.41583
8722670	Lake Worth Pier	-80.034167	26.61277

Table 2 Information of NOAA CO-OPS stations on Gulf of Mexico coast

Station ID	Station Name	Longitude	Latitude
8723970	Vaca Key	-81.1065	24.711
8725110	Naples Gulf of Mexico	-81.8075	26.13166
8725520	Fort Myers	-81.871	26.648
8726384	Port Manatee	-82.5625	27.63833
8726520	Tampa Bay	-82.626944	27.76111
8726607	Old Port Tampa	-82.552803	27.8578
8726667	Mckay Bay Entrance	-82.425003	27.9133
8726724	Clearwater Beach	-82.831667	27.97833
8727520	Cedar Key	-83.0317	29.135
8728690	Apalachicola	-84.980556	29.72444
8729108	Panama City	-85.664444	30.14972
8729210	Panama City Beach	-85.878583	30.21375
8729840	Pensacola	-87.211197	30.4044
8732828	Weeks Bay Mobile Bay	-87.825401	30.41690
8735180	Dauphin Island	-88.075	30.25
8735391	Dog River Bridge	-88.088056	30.56527
8735523	East Fowl River Bridge	-88.113899	30.44370
8736897	Coast Guard Secto Mobile	-88.058111	30.6495
8737048	Mobile State Docks	-88.03961	30.70461
8737138	Chickasaw Creek	-88.07361	30.7819
8738043	West Fowl River Bridge	-88.1586	30.3766
8739803	Bayou La Batre Bridge	-88.247806	30.40625
8741533	Pascagoula NOAA Lab	-88.563056	30.36777
8747437	Bay Waveland Yacht Club	-89.3258	30.32634
8760721	Pilottown	-89.258833	29.17930
8760922	Pilots Station East S.W. Pass	-89.4075	28.93222
8761305	Shell Beach	-89.673	29.8683
8761724	Grand Isle	-89.956667	29.26333
8762075	Port Fourchon Belle Pass	-90.199167	29.11416

8764227	Lawma Amerada Pass	-91.338097	29.4496
8766072	Freshwater Canal Locks	-92.305194	29.55169
8767816	Lake Charles	-93.221667	30.22361
8767961	Bulk Terminal	-93.300697	30.1903
8768094	Calcasieu Pass	-93.342889	29.76816
8770475	Port Arthur	-93.93	29.86669
8770520	Rainbow Bridge	-93.884694	29.98119
8770570	Sabine Pass North	-93.8701	29.7284
8770613	Morgans Point, Barbours Cut	-94.985	29.68166
8770777	Manchester	-95.2658	29.72629
8770822	Texas Point Sabine Pass	-93.841797	29.68930
8771013	Eagle Point Galveston Bay	-94.917253	29.48130
8771341	Galveston Bay	-94.724725	29.35746
8771450	Galveston Pier	-94.793306	29.31
8771972	San Luis Pass	-95.130833	29.08055
8772447	Freeport	-95.3025	28.94330
8775870	Bob Hall Pier Corpus Christi	-97.2167	27.58
8779770	Port Isabel	-97.215528	26.06116

3.2 Non-tidal elevation

The non-tidal elevation is assessed using a low-pass filter with a 2-day cutoff. Fig. 6 illustrates the spatial distribution of mean RMSE and bias. Approximately 80% of the stations exhibit an RMSE of less than 10 cm. Stations with higher RMSE values are predominately located in inland Louisiana and Chesapeake Bay. In addition, inland stations in Louisiana show a significant positive bias, whereas Chesapeake Bay stations display a substantial negative bias (Fig. 6b).

Fig. 7 shows the comparisons, grouped into 7 regions: Gulf of Maine (Fig. 7a), Atlantic coast south of Gulf of Maine (Fig. 7b), Florida (Fig. 7c), east Gulf of Mexico (Fig. 7d), west Gulf of Mexico (Fig. 7e), inland stations along the east coast (Fig. 7f), and inland stations along Gulf of Mexico (Fig. 7g). Several stations (especially inland stations) are outside the VDatum coverage, so both model and observation are de-meaned at those stations to remove the model bias. At other stations, the observation is converted to xGEOID20b before the comparison, and no further datum adjustment is made. Our assessment therefore constitutes a rigorous validation for both non-tidal and TWL. The seasonal variations for the non-tidal water level are coherent in each region, suggesting a synoptic scale response. The model well reproduces the inter-seasonal variations and strong weather events, as evidenced by a high overall correlation coefficient of 0.83. For example, a storm surge on the Atlantic coast (Fig. 7b and 7f) occurred in early October 2015, driven by Hurricane Joaquin. Cold front events usually prevail along the Gulf Coast between October and April (Feng and Li, 2010) and the model successfully captures the larger water level swings induced by the cold front events as compared to calmer summer months (Fig. 7d, 7e, and 7g). The mean bias and RMSE for the non-tidal elevations at all NOAA stations (including inland stations) are -1.2 cm and 9.2 cm, respectively, both quite good considering the

large variability. In contrast, RMSE for v4 is 11.9 cm. This is a major improvement over some barotropic models, which are unable to capture the non-tidal signals well (cf. Section 4.1).

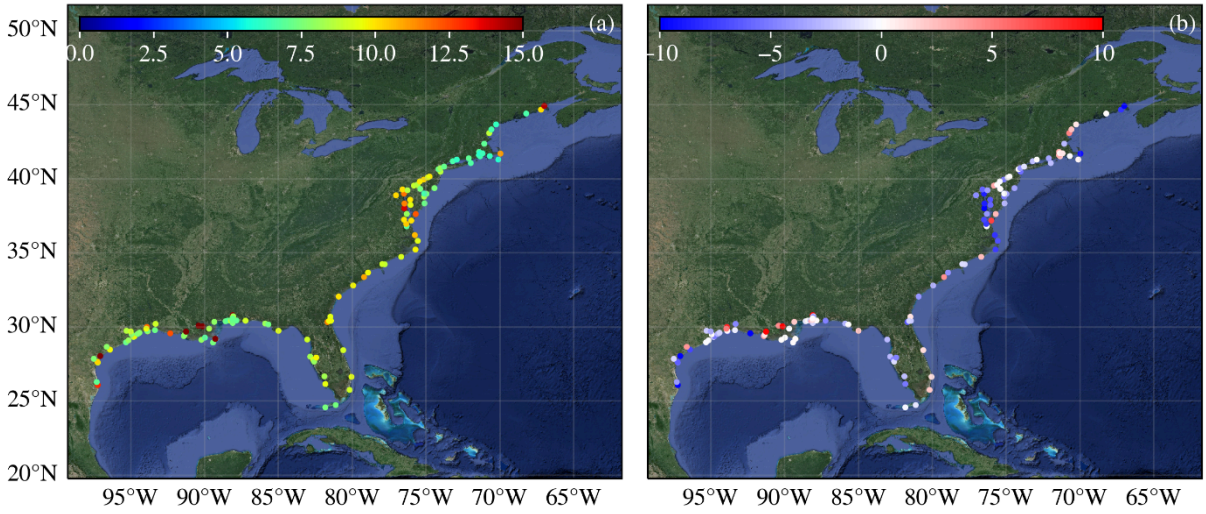

Fig. 6: Distribution of (a) RMSE (in cm) and (b) bias (in cm) for non-tidal water level from a full-year simulation.

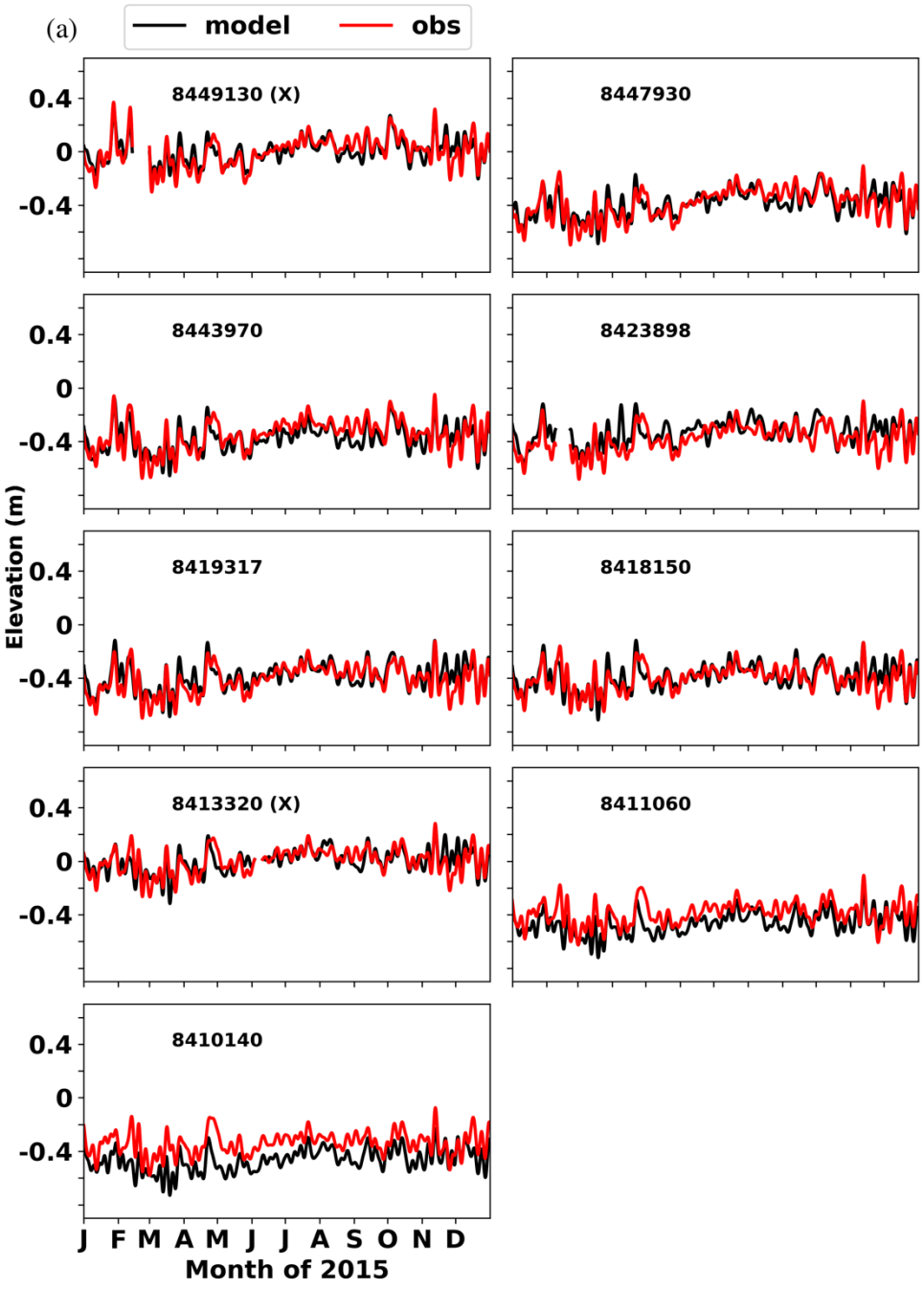
(a)
model
obs
8449130 (X)
8447930
8443970
8423898
8419317
8418150
8413320 (X)
8411060
8410140
0.4
0
-0.4
Elevation (m)
J F M A M J J A S O N D
Month of 2015

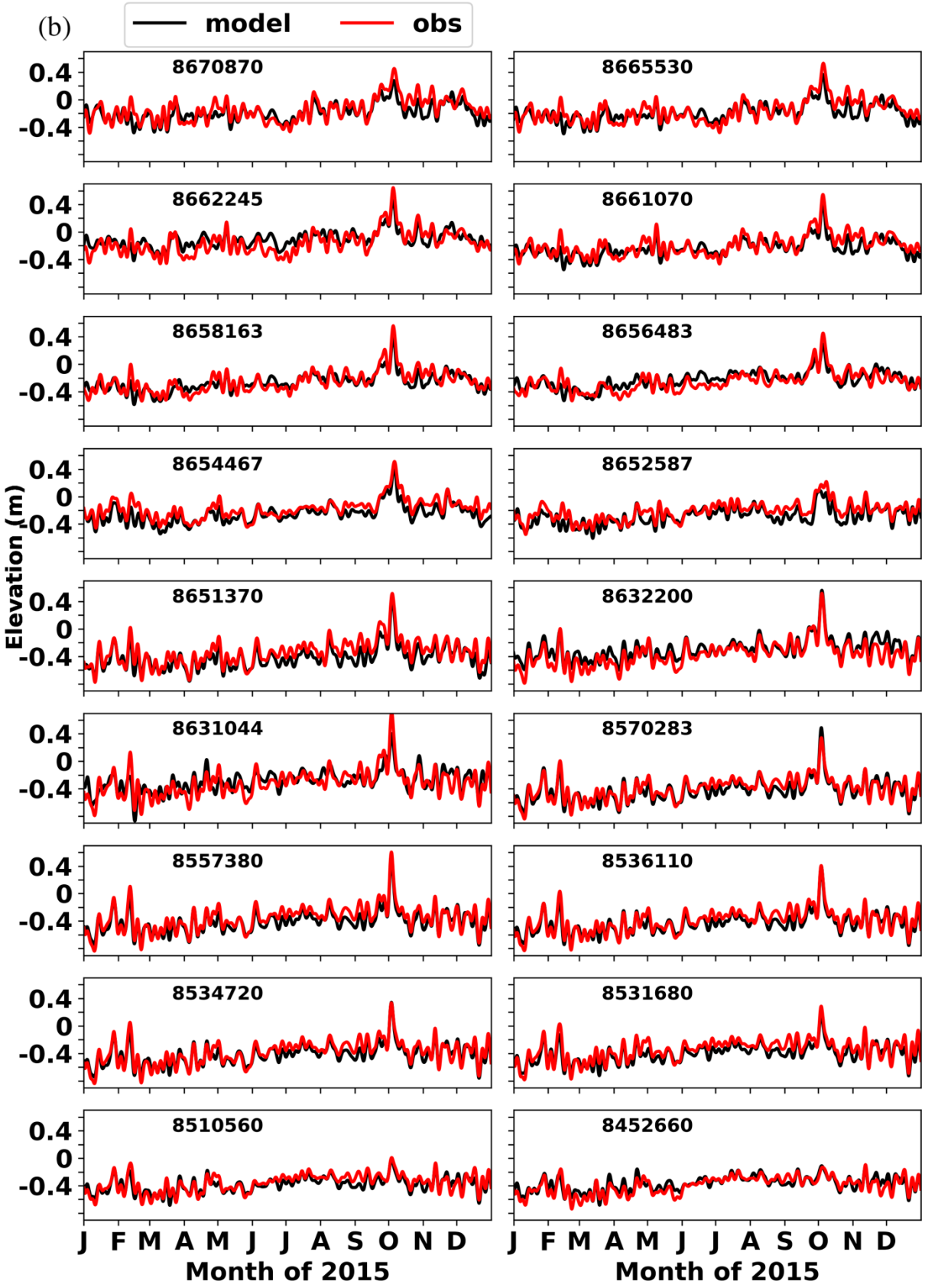
(b)
model
obs
8670870
8665530
8662245
8661070
8658163
8656483
8654467
8652587
8651370
8632200
8631044
8570283
8557380
8536110
8534720
8531680
8510560
8452660
0.4
0
-0.4
Elevation (m)
J F M A M J J A S O N D
Month of 2015

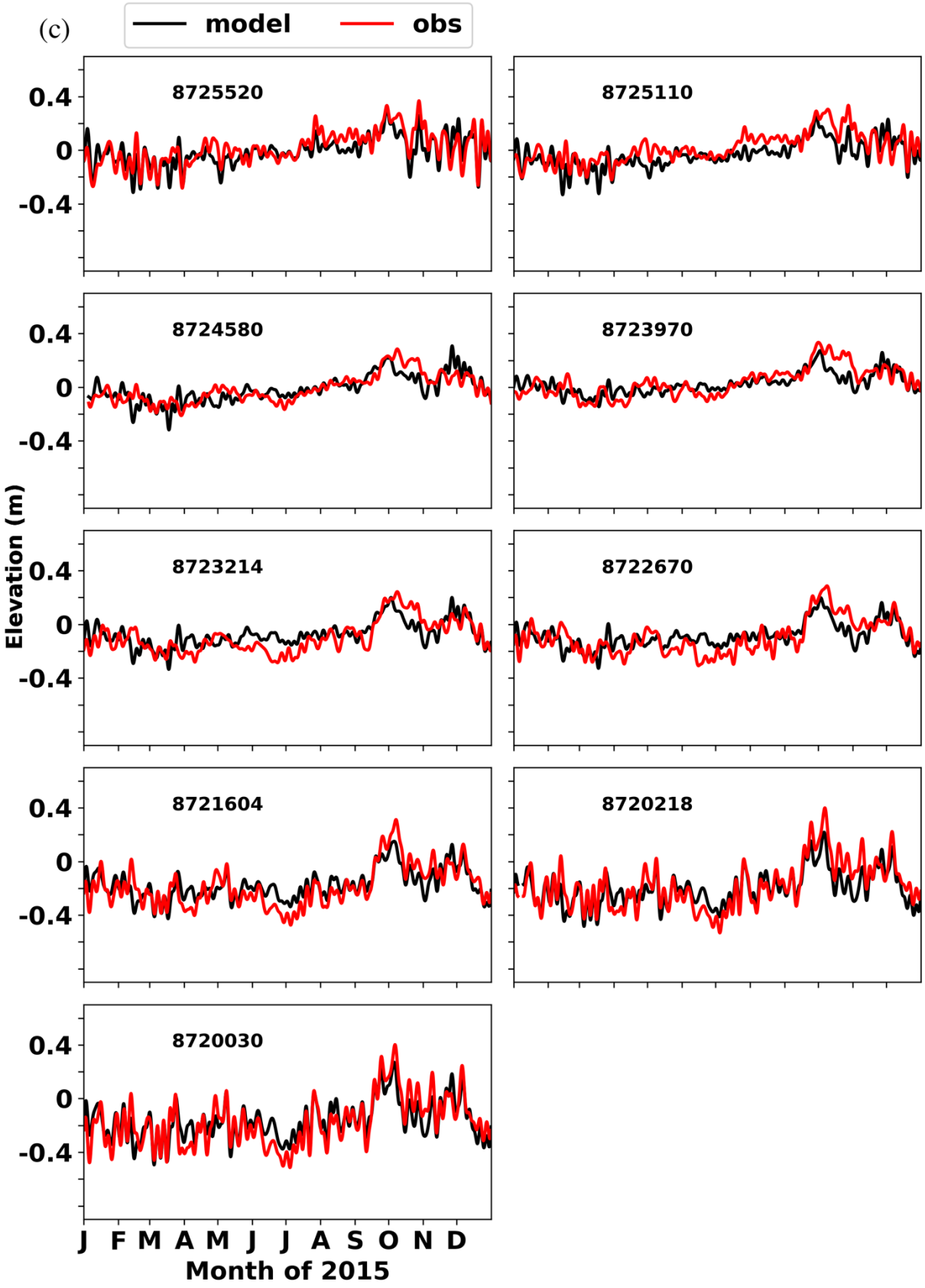
(c)
model
obs
8725520
8725110
8724580
8723970
8723214
8722670
8721604
8720218
8720030
0.4
0
-0.4
Elevation (m)
J F M A M J J A S O N D
Month of 2015

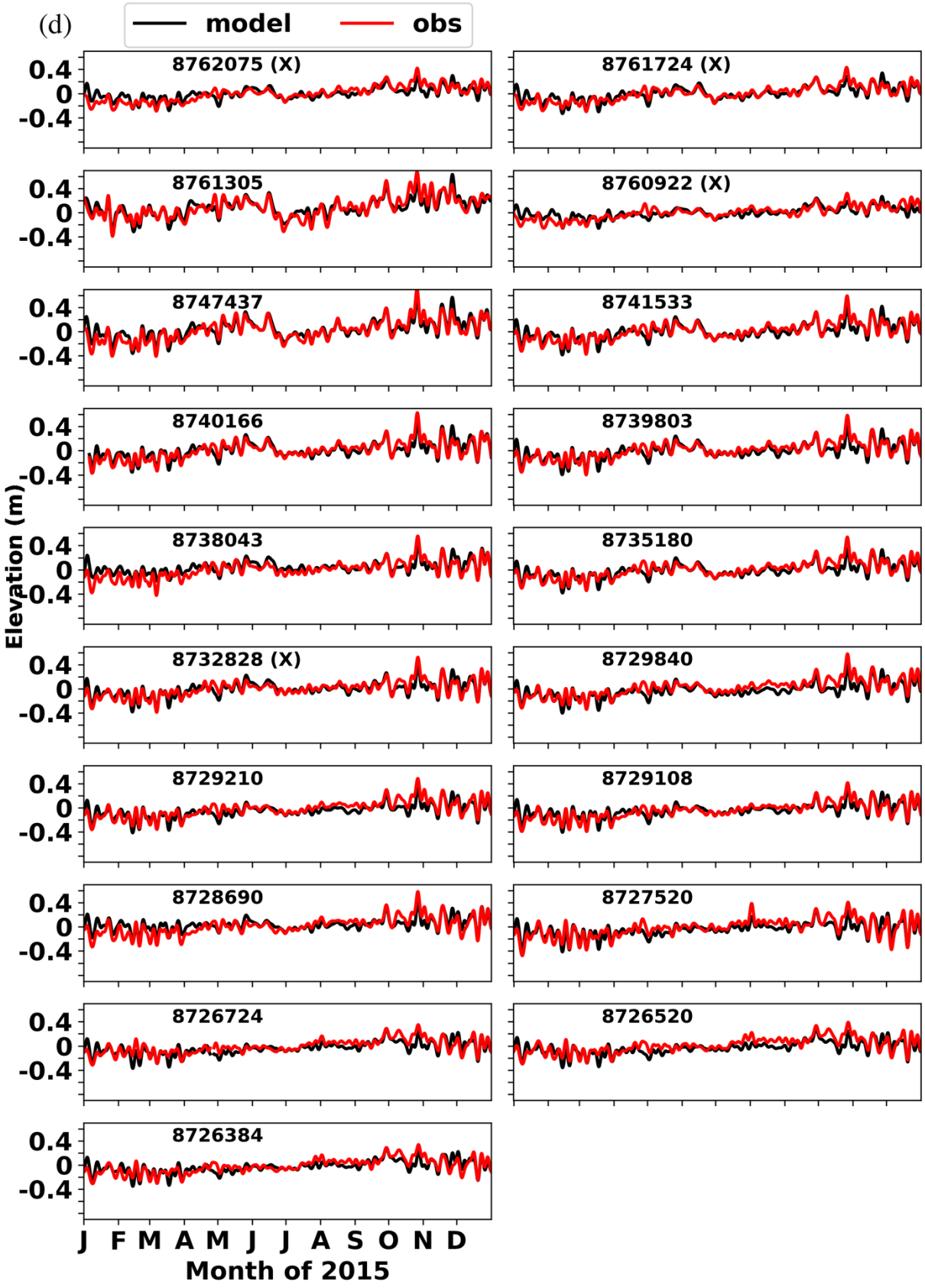
(d)
model
obs
8762075 (X)
8761724 (X)
8761305
8760922 (X)
8747437
8741533
8740166
8739803
8738043
8735180
8732828 (X)
8729840
8729210
8729108
8728690
8727520
8726724
8726520
8726384
0.4
0
-0.4
Elevation (m)
J F M A M J J A S O N D
Month of 2015

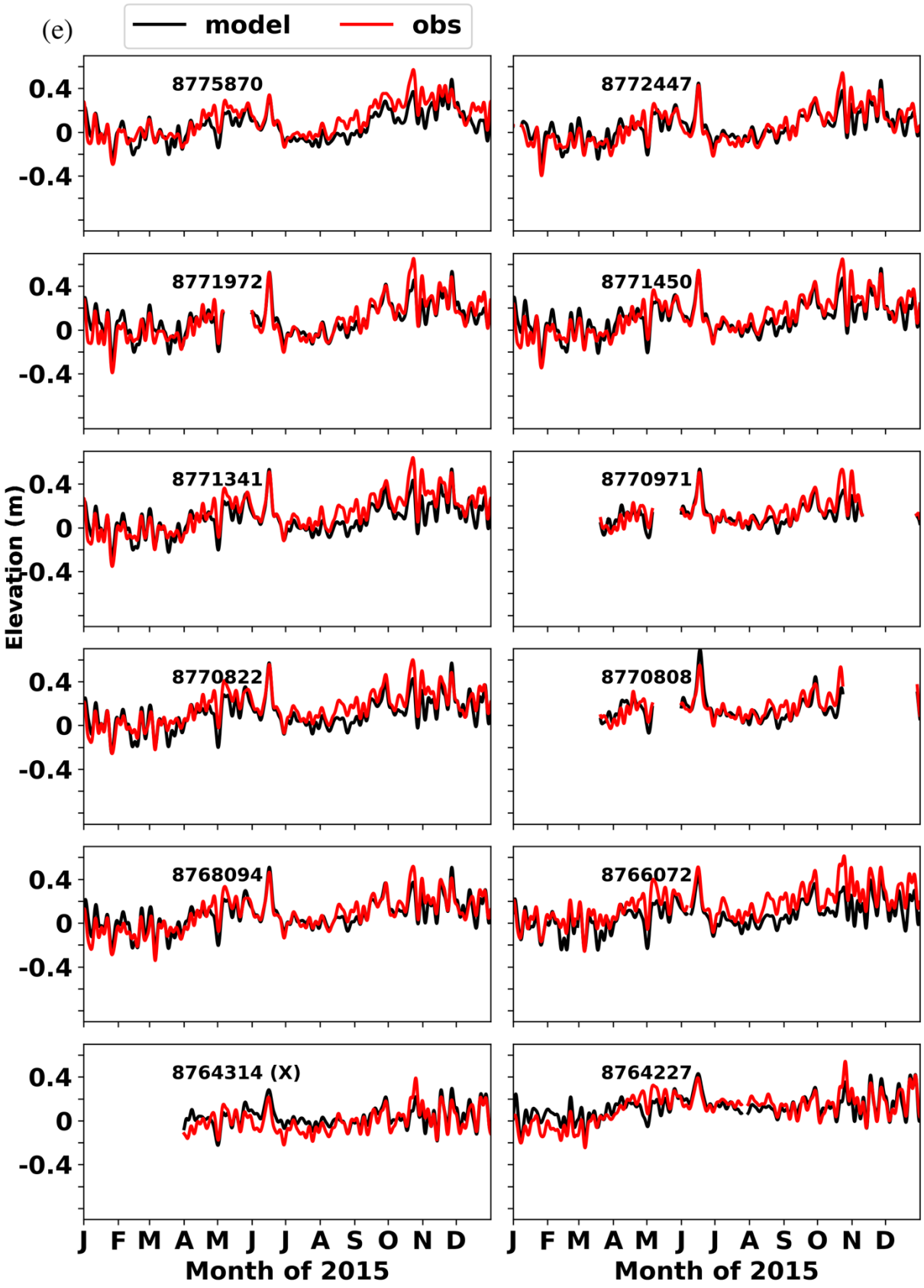
(e)
model
obs
8775870
8772447
8771972
8771450
8771341
8770971
8770822
8770808
8768094
8766072
8764314 (X)
8764227
0.4
0
-0.4
Elevation (m)
J F M A M J J A S O N D
Month of 2015

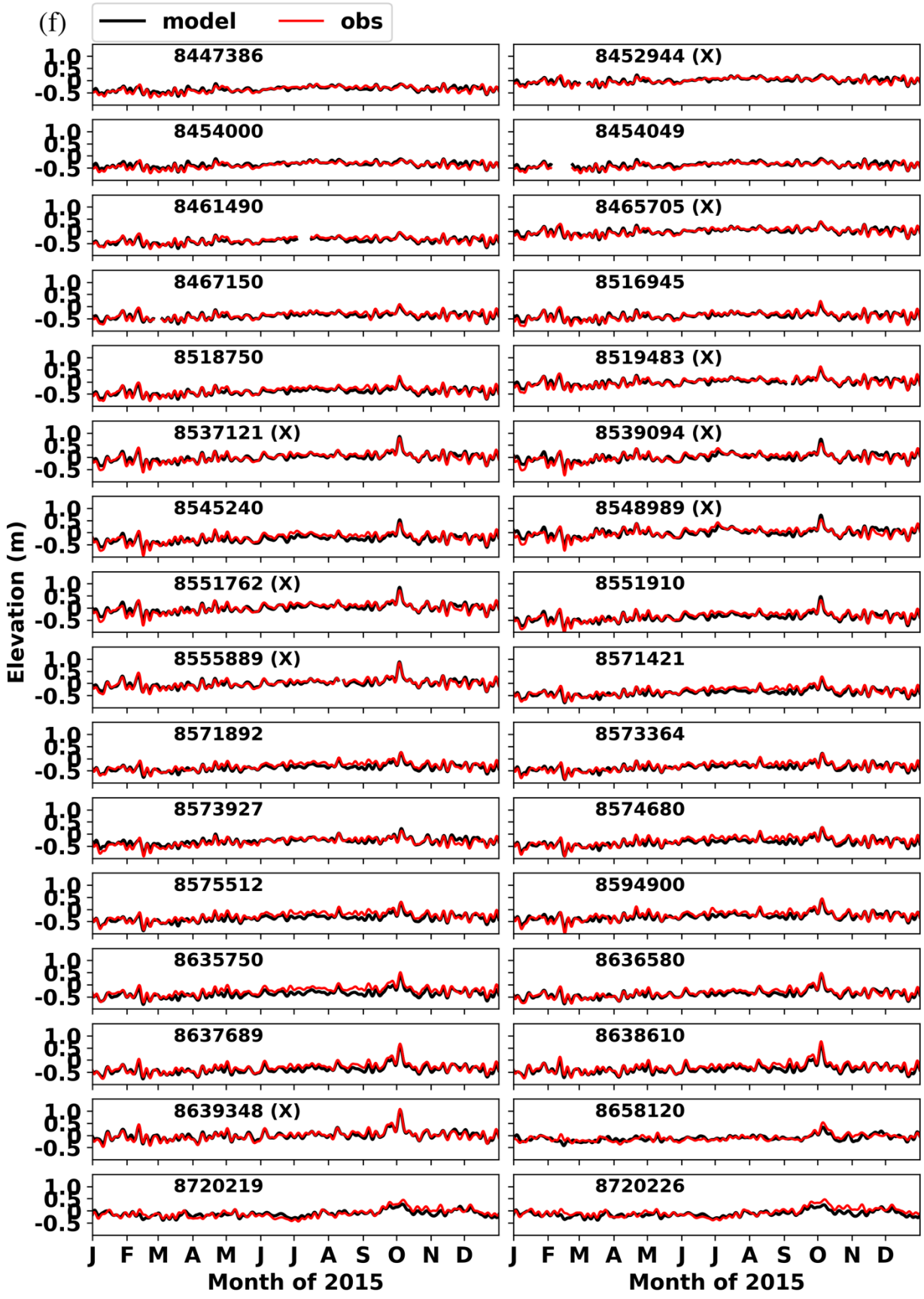
(f)
model
obs
8447386
8452944 (X)
8454000
8454049
8461490
8465705 (X)
8467150
8516945
8518750
8519483 (X)
8537121 (X)
8539094 (X)
8545240
8548989 (X)
8551762 (X)
8551910
8555889 (X)
8571421
8571892
8573364
8573927
8574680
8575512
8594900
8635750
8636580
8637689
8638610
8639348 (X)
8658120
8720219
8720226
1.0
0.5
0.0
-0.5
Elevation (m)
J F M A M J J A S O N D
Month of 2015

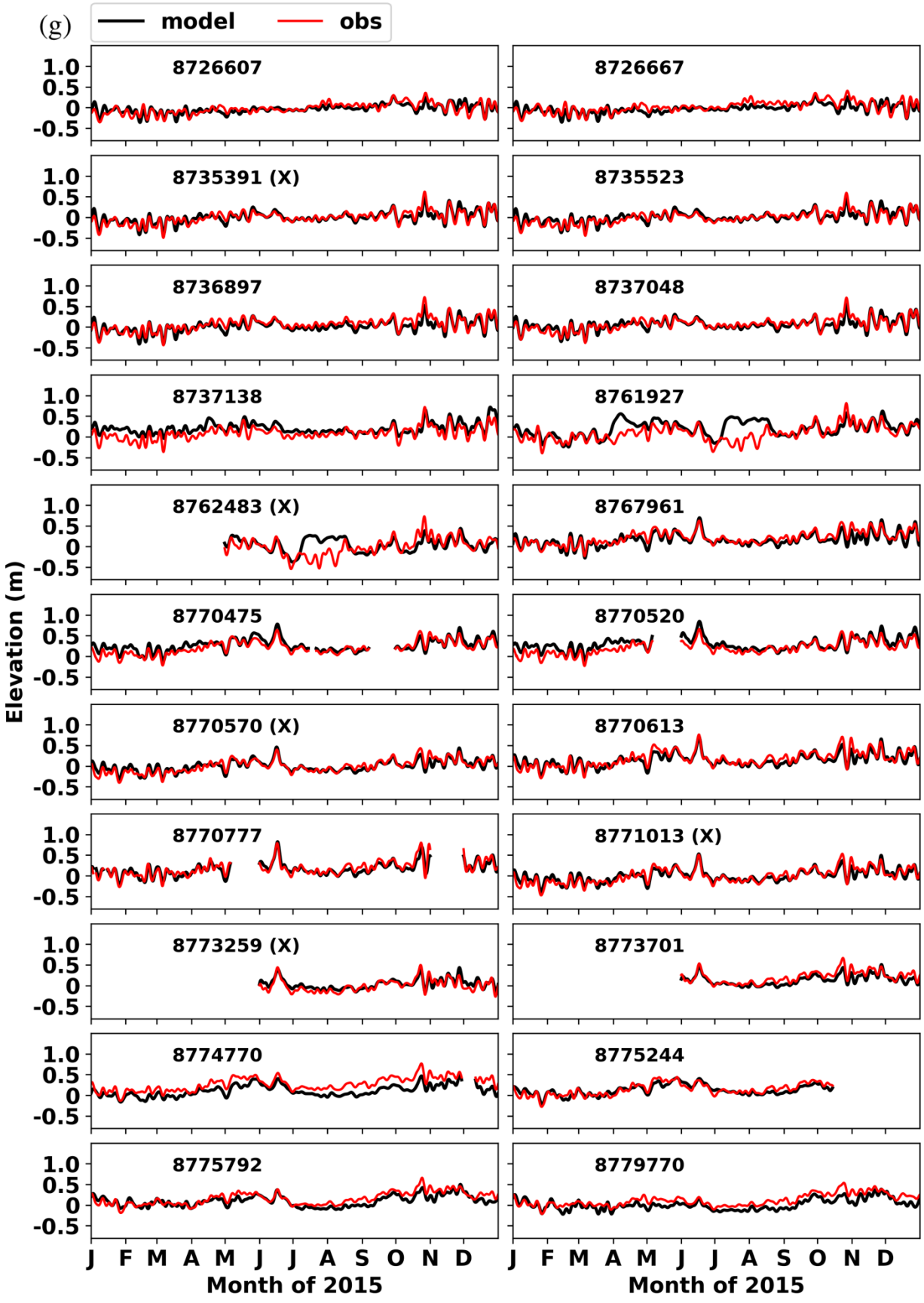
(g)
model
obs
8726607
8726667
8735391 (X)
8735523
8736897
8737048
8737138
8761927
8762483 (X)
8767961
8770475
8770520
8770570 (X)
8770613
8770777
8771013 (X)
8773259 (X)
8773701
8774770
8775244
8775792
8779770
Elevation (m)
1.0
0.5
0
-0.5
J F M A M J J A S O N D
Month of 2015

Fig. 7: Comparison of low pass filtered water elevations at NOAA CO-OPS stations. The observation has been converted to xGEOID20b at most stations; datum conversion at the stations marked with "X" is not available so both observation and model are de-meaned. The gaps at some stations are due to missing data. (a) Gulf of Maine; (b) Atlantic coast south of Gulf of Maine; (c) Florida; (d) east Gulf of Mexico; (e) west Gulf of Mexico; (f) inland stations along US east coast; (g) inland stations along the Gulf of Mexico.

3.3 Total water levels

The model's ability to accurately simulate the tidal and non-tidal elevations as shown in the previous two sub-sections bodes well for the TWL. The correlation coefficient (CC), bias, and RMSE for TWL averaged over all NOAA stations (including the inland stations) are 0.89, -1.8± 4.5 cm, and 14.0 cm, respectively. In contrast, RMSE for v4 is 16.9 cm. Fig. 8 shows the spatial distribution of mean RMSE and bias. Larger RMSEs are found in the macro-tidal regions, i.e., New England coast, and some inland areas where the DEM quality is highly questionable (Fig. 8). 74% of all stations have an absolute bias below 5 cm. Stations with large negative bias are found in Chesapeake Bay, whereas stations with large positive bias are in the watershed of Louisiana (which happens to be the area with highest uncertainty in xGEOID20b) (Fig. 8b). Representative comparisons are shown in Fig. 9, for stations along the east coast (Fig. 9a) and Gulf coast (Fig. 9b). Both amplitude and phase at most stations are well simulated, together with the spring/neap tidal cycle and non-tidal fluctuations. It seems sufficient to apply only eight tidal constituents at the ocean boundary as it is located far away from the coast and FES2014 is sufficiently accurate there. Using ADT to drive the model at the ocean boundary significantly improves the TWL. Compared to STOFS3D-v4, the adjustment procedure at the ocean boundary made in 'v6' is very simple: in 'v4' we had to impose a non-uniform adjustment to compensate for the errors in the non-tidal elevations, whereas a uniform adjustment is sufficient in 'v6'.

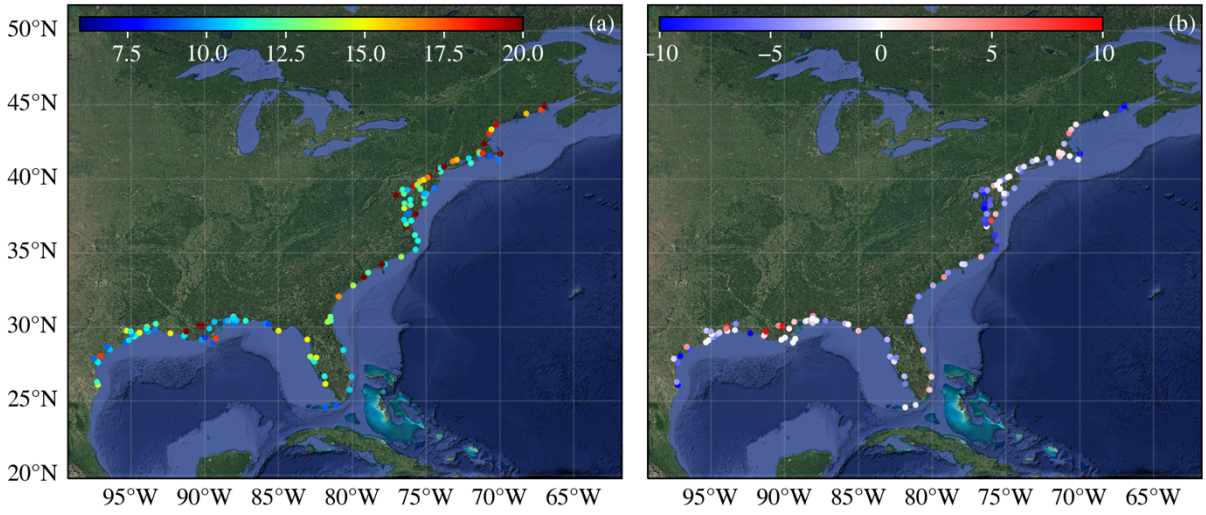

Fig. 8: Distribution of (a) RMSE (in cm) and (b) bias (in cm) for TWL from a full-year simulation.

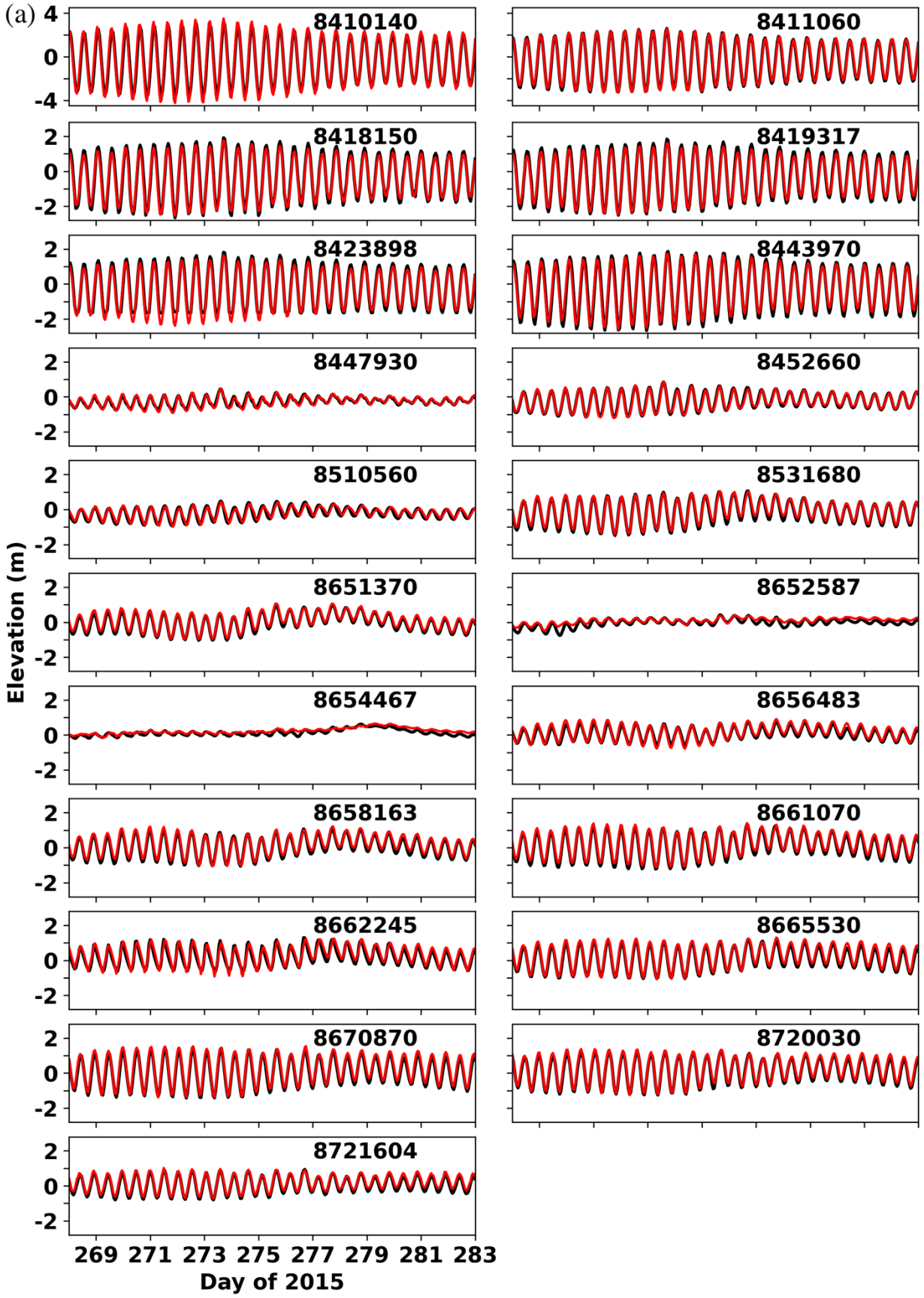
(a)
8410140
8411060
8418150
8419317
8423898
8443970
8447930
8452660
8510560
8531680
8651370
8652587
8654467
8656483
8658163
8661070
8662245
8665530
8670870
8720030
8721604
Elevation (m)
269 271 273 275 277 279 281 283
Day of 2015

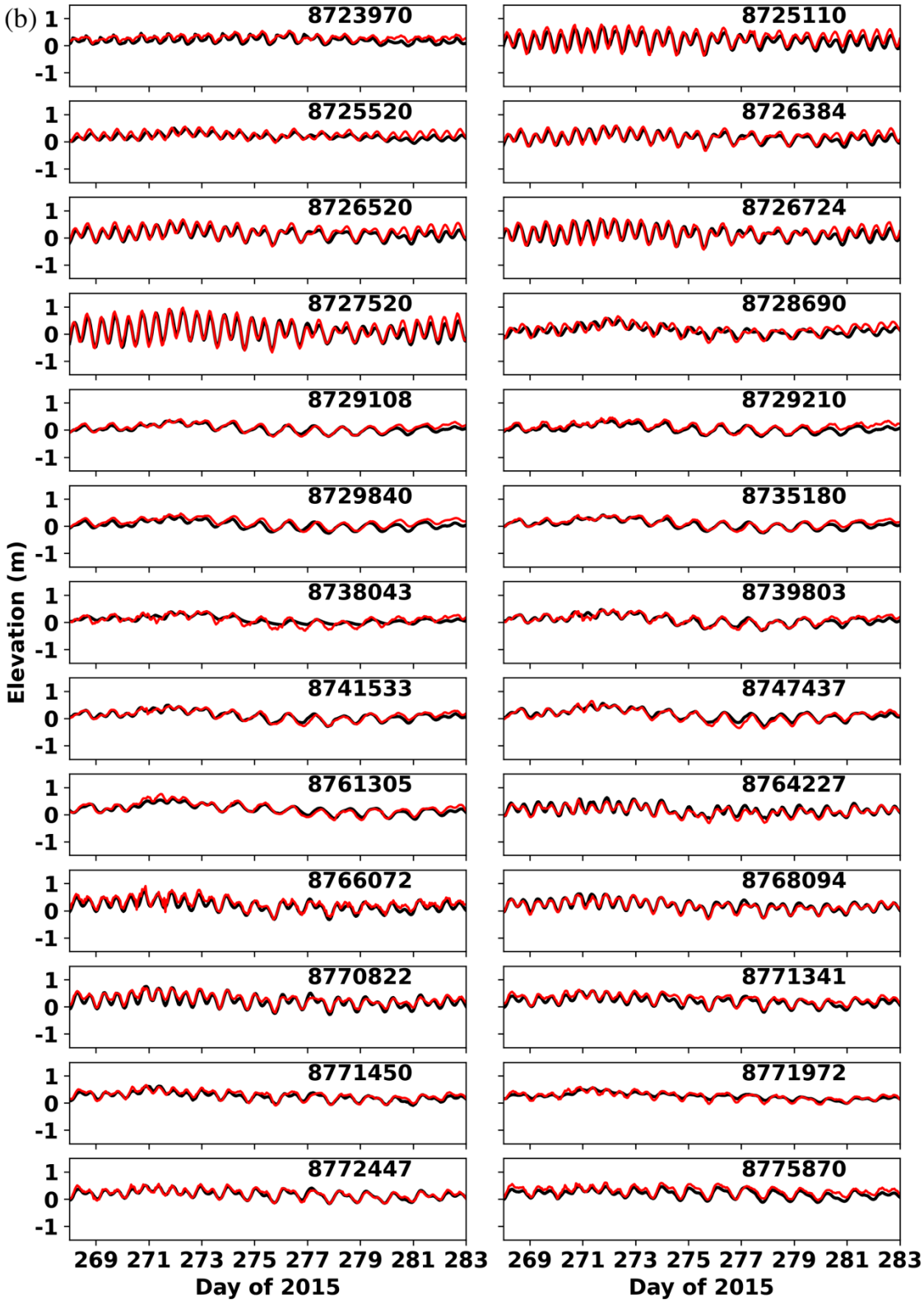
(b)
8723970
8725110
8725520
8726384
8726520
8726724
8727520
8728690
8729108
8729210
8729840
8735180
8738043
8739803
8741533
8747437
8761305
8764227
8766072
8768094
8770822
8771341
8771450
8771972
8772447
8775870
Elevation (m)
1
0
-1
269 271 273 275 277 279 281 283
Day of 2015

Fig. 9: Sample comparisons of total water elevation at some NOAA CO-OPS stations. (a) U.S. east coast stations. Note that the *y*-axis range for the first row is [-4.5, 4.5], but is [-2.8, 2.8] for other rows. (b) Gulf coast stations; the *y*-axis range is [-1.5, 1.5].

Fig. 10 shows the comparison of yearly (2015) averaged dynamic topography between the model and AVISO/ADT. Generally, the model well reproduces the coastal water levels (where AVISO may also have some uncertainty), especially the Atlantic coast and eastern Gulf of Mexico coast. At the ocean boundary, the two are essentially the same because the non-tidal boundary condition we used is derived from AVISO. The position of the 10-cm contour line from the model is close to that from AVISO from Florida Keys to Cape Hatteras. However, the model shows discrepancies in the separation of Gulf Stream and the shedding of Loop current eddies. For example, the model exaggerates the meanders near Cape Hatteras, which pushes the position of Gulf Stream further north. This may be due to a weaker Gulf Stream in the model. Another reason may be related to the model errors in the Loop Current (Andres 2021). The free meandering part of the Gulf Stream is also different from AVISO. Without data assimilation, model errors inevitably grow over time and the model needs to be re-initialized after 1 year to prevent long-term drift.

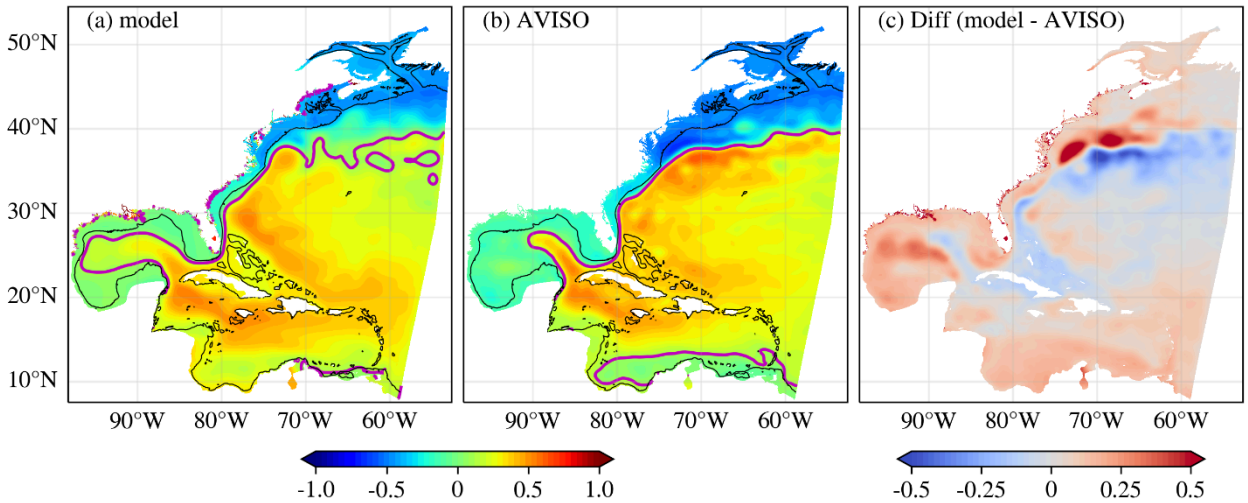

Fig. 10: Yearly averaged dynamic topography (unit: m) for (a) model, (b) AVISO/ADT (adjusted by -0.42 m), and (c) difference between model and AVISO. The magenta line is the 10-cm contour line, the black solid line is the 200-m isobath. For comparison, AVISO ADT was interpolated into model's grid.

3.4 Model evaluation for surface currents

Daily averaged surface currents are compared with observations from CODAR near the end of the simulation. To this end, four U.S. coastal regions with high data availability (for proper averaging in space and time) were selected, including the mid-Atlantic coast near Chesapeake Bay, Mississippi Sound, Tampa Bay, and New York/New Jersey (NY/NJ) coast. Both model and observation were daily averaged, and model velocities were interpolated onto the observation grid. Figs. 11-14 show the comparison of mean surface currents in November 2015 (near the end of the simulation) in these regions; note that observation availability varies in each region. Overall, the model reproduces the surface circulation but overestimates the velocity magnitude in some areas. In November, the surface currents along the Atlantic coast are dominated by southwestward currents driven by northeasterly wind, while Gulf Stream is dominant near the

shelf break. The modeled and observed surface currents show consistency in the inner shelf from Chesapeake Bay to Delaware Bay (Fig. 11). However, the simulated Gulf Stream's exit point near Cape Hatteras was estimated farther north than the observation, which is consistent with the ADT comparison. As a result, larger currents were generated over the outer shelf, which also affected the currents over the shelf near NY/NJ coast (Fig. 12). In Mississippi Sound (Fig. 13) and Tampa Bay (Fig. 14), the modeled currents were generally correct in direction but overpredicted the magnitude in some areas. Comprehensive validation of surface and sub-surface currents is on-going but overall, the model skill for the surface currents is satisfactory given the fact that no data assimilation was used.

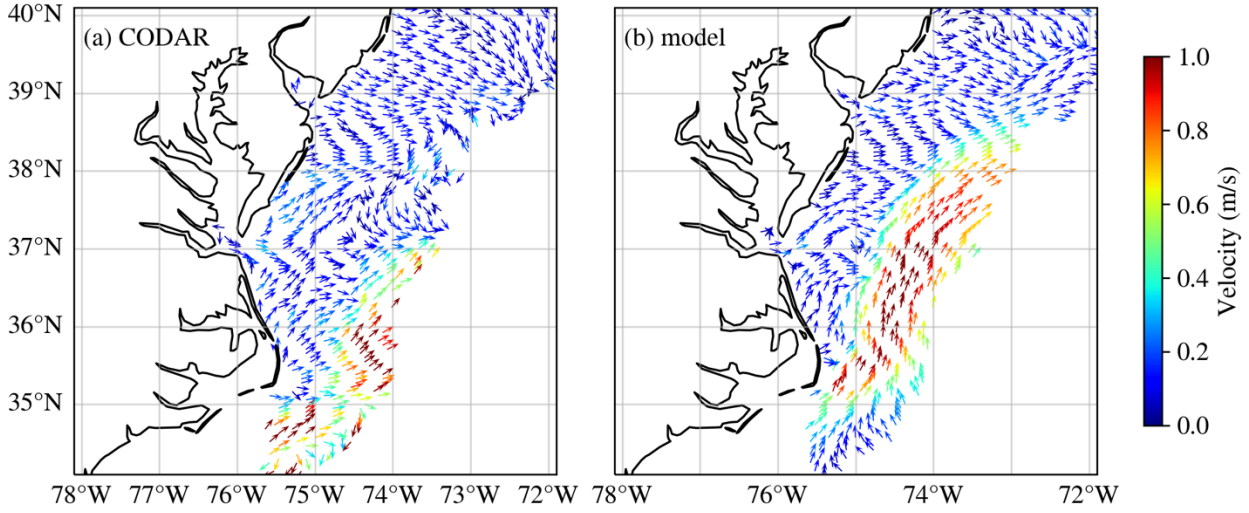

Fig. 11: Comparison of daily averaged surface currents on November 16, 2015, from (a) CODAR, (b) model results over the Mid-Atlantic coast.

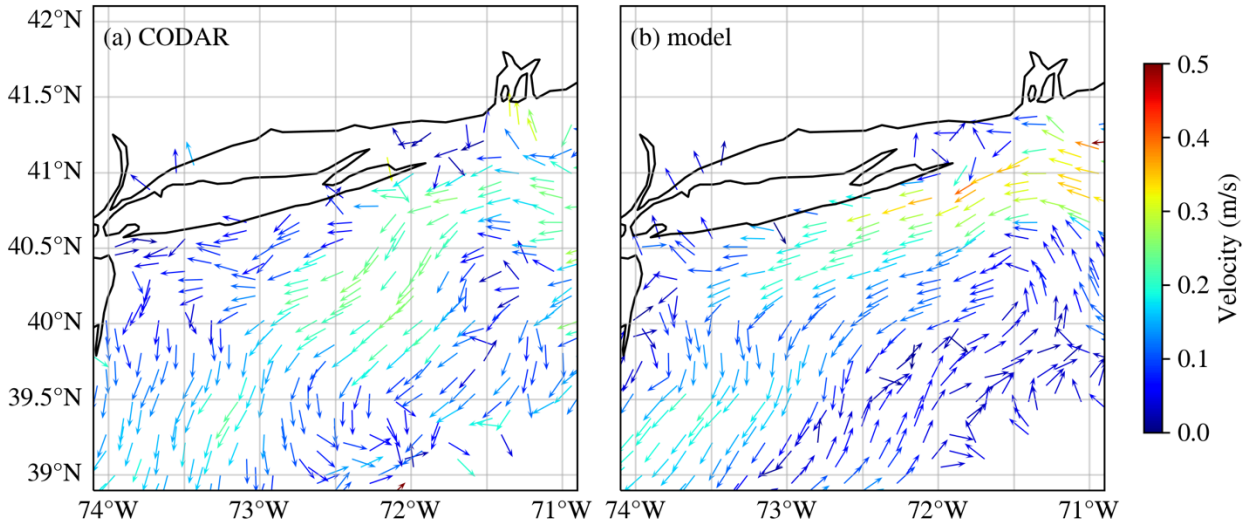

Fig. 12: Comparison of daily averaged surface currents on November 12, 2015, from (a) CODAR, (b) model results near NJ/NY coast.

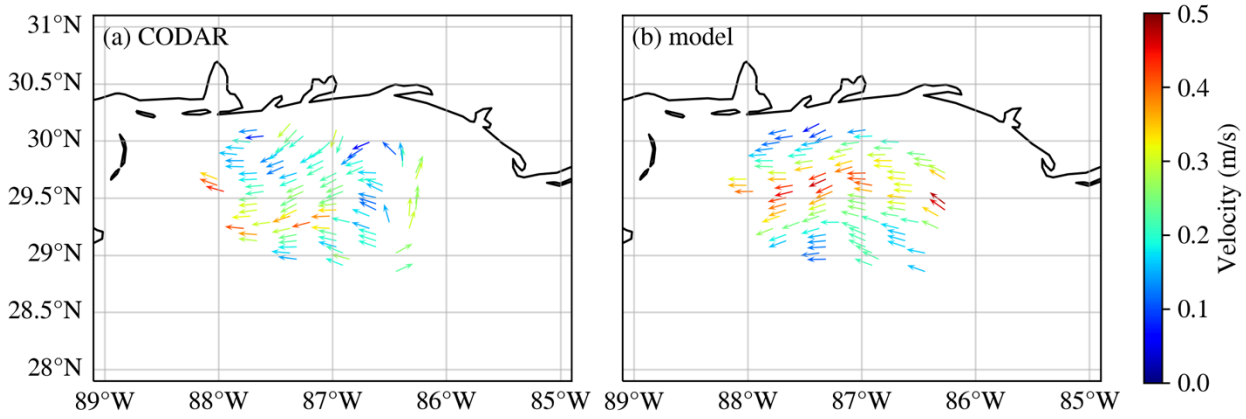

Fig. 13: Comparison of daily averaged surface currents on November 20, 2015, from (a) CODAR, (b) model results near Mississippi Sound.

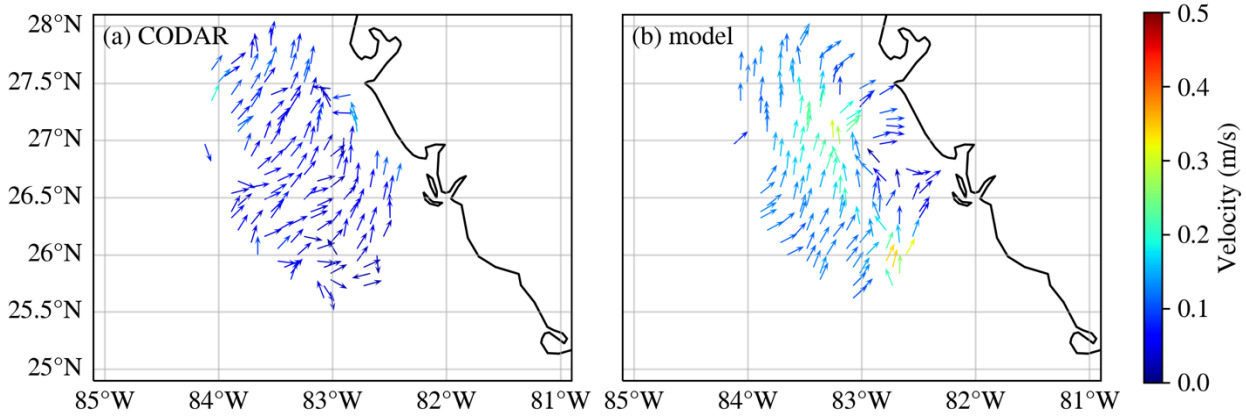

Fig. 14: Comparison of daily averaged surface currents for November 9, 2015, from (a) CODAR, (b) model results near Tampa Bay.

4. Discussions

Many sensitivity simulations have been conducted for this large domain, and for brevity we will focus on two important aspects on the boundary effects and the thermohaline steric effects. The focus of this paper is on water level, which is much easier to calibrate than 3D variables like currents, temperature and salinity. Validation of 3D variables, especially in coastal regime requires site-specific considerations like bottom roughness and turbulence mixing regimes. Principles on defensible coastal modeling that are centered around faithful DEM representation are elucidated in Zhang et al. (2024).

4.1 Thermohaline steric effects

The non-tidal elevations are primarily driven by atmospheric forcing and steric effects. Frederikse et al. (2017) find that, after adjusting for local atmospheric effects and smoothed on decadal timescales, sea level changes from a tide gauge north of Cape Hatteras over 1965-2014 are correlated with upper-ocean steric height changes in the Labrador Sea and the deep midlatitude North Atlantic inter-gyre region. Storto et al. (2019) showed that the tide gauges on

the east coast of U.S. exhibit significant correlations (> 0.6) with the ensemble mean steric sea level.

The 3D baroclinic model used here already incorporates the thermohaline steric effects (due to uneven mass distribution of the ocean); using the ADT to drive the model also helps to capture part of other types of steric effects (e.g., thermal expansion due to the non-Boussinesq effect) even though these effects are not included in the model physics; obviously, the constant offset applied at the ocean boundary (Section 2.3) affects the results also. As a result, the non-tidal elevations are well simulated.

A known issue plaguing barotropic models is their inability to capture the thermohaline steric effects, resulting in underestimation of seasonal and annual variability in the simulated non-tidal elevations. As far as modeling is concerned, a frequently asked question is whether a barotropic model can capture the steric effects with some tweaking in the boundary condition. This is tested here with a 3D barotropic model based on the 3D baroclinic model used in this paper, with baroclinic gradient neglected, and a uniform offset is applied to the boundary condition. Different offsets are tested to minimize the model error. However, Figs. 15 and 16 clearly indicate that this strategy does not work for large domains like ours as the biases vary both in time and space, making it difficult to compensate with boundary condition adjustment. For example, the barotropic model bias ranges from 10cm to 30cm, and is generally higher in the south (especially in Florida) than in the north along the east coast. In the Gulf coast, the bias is highly variable but is generally larger than 20 cm. On the other hand, the 3D baroclinic model can accurately capture the seasonal and event-scale variabilities with a simple boundary condition.

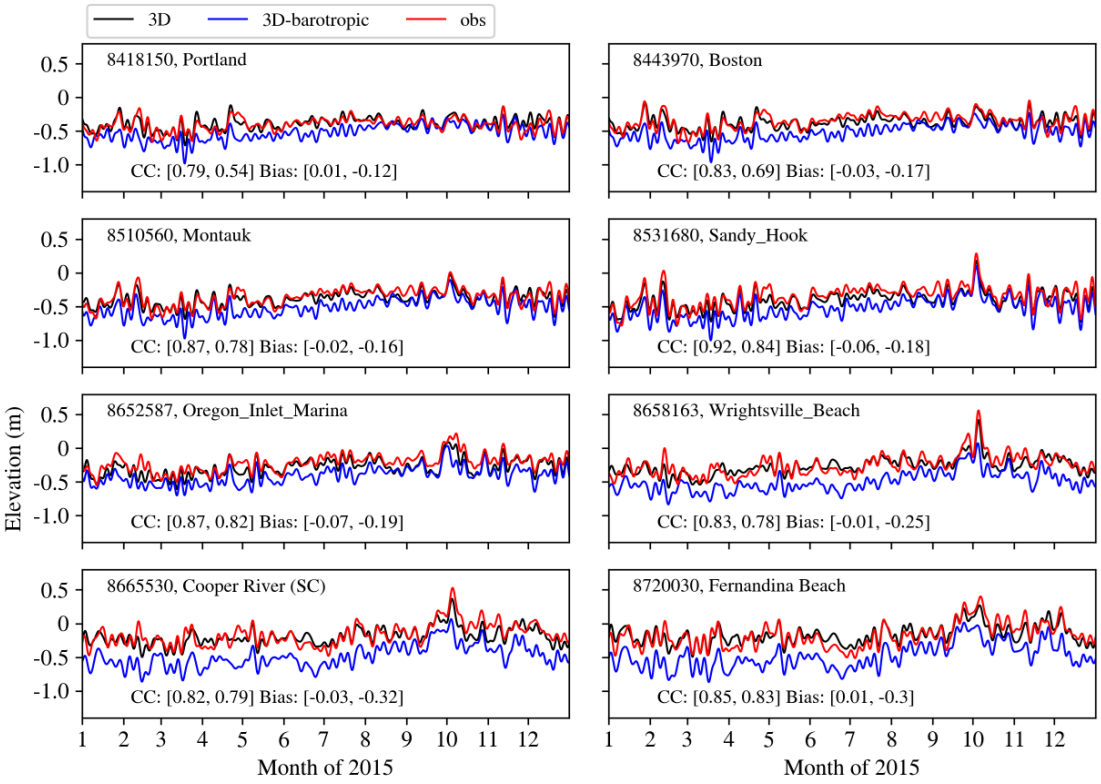

Fig. 15: Comparison of non-tidal elevations from 3D baroclinic and 3D barotropic simulations at some representative NOAA stations along the east coast. Correlation coefficient (CC) and averaged bias are shown in panel, with the first number for the 3D-baroclinic model and the second number for the 3D-barotropic model.

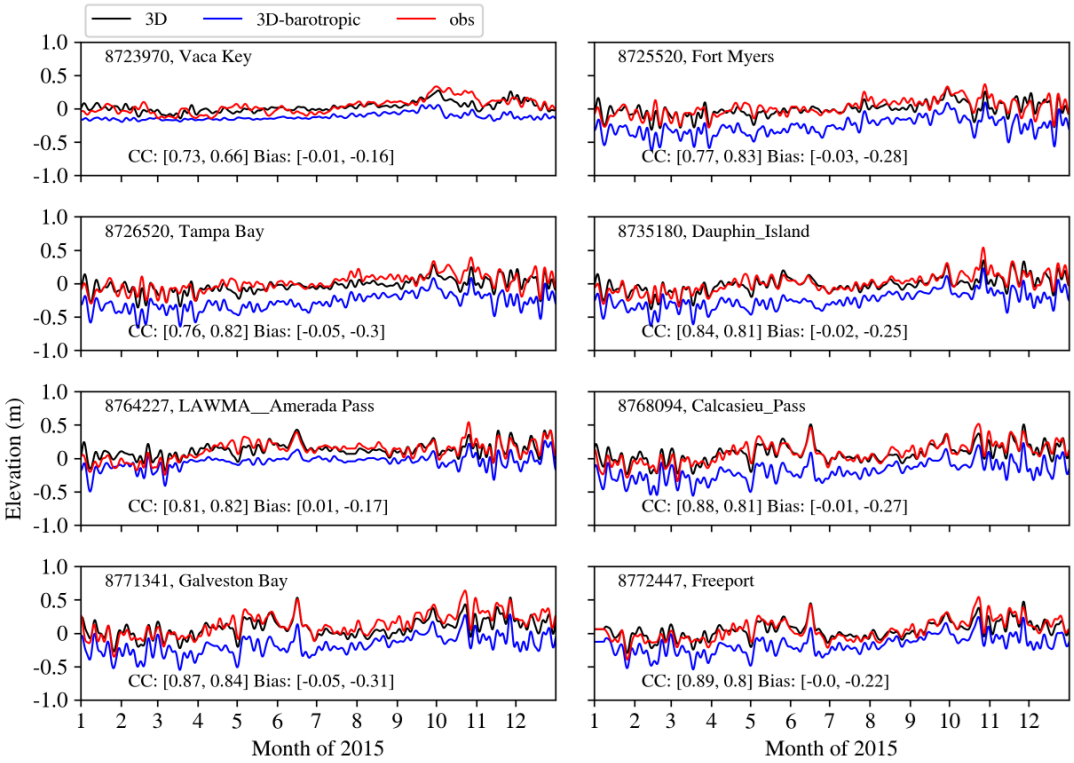

Fig. 16: Same as Fig. 15 but for NOAA stations along the Gulf of Mexico coast.

4.2 Remote forcing for the non-tidal water level variability in the Gulf of Maine

Our early numerical experiment results revealed a large sensitivity of the non-tidal elevation in the Gulf of Maine to the ocean boundary location. The ocean boundary used in STOFS3D-v4 is located at 60°W, and thus its domain excludes Gulf of St. Lawrence and its influence. The Gulf of Maine connects with the Gulf of St. Lawrence via the Scotian Shelf. The mean surface current on the Scotian Shelf is about 0.1 m/s; fresh water from the Gulf of St. Lawrence enters the eastern Scotian Shelf through Cabot Strait, and then moves southwestward as the Nova Scotian Current (~0.3 m/s), and finally enters the Gulf of Maine at Cape Sable (Sheng et al., 2001). To demonstrate this important remote connection, a sensitivity test was conducted by using v4's mesh with v6's setup otherwise. The comparison of sub-tidal water levels for stations in the Gulf of Maine is shown in Fig. 17. The variability is similar among the seven stations, which is mostly driven by synoptic weather systems (2 – 10 days). STOFS3D-v6, with the Gulf of St. Lawrence included, better reproduces the synoptic water level variability in April but overpredicts the set-down in May. Compared with v6, results from the v4 mesh consistently show large negative bias in the non-tidal signal, thus suggesting a strong influence from the boundary; particularly, the simulated Nova Scotian Current in 'v6' helps to raise the water level in Gulf of Maine via the geostrophic adjustment. With Gulf of St. Lawrence excluded, the velocity boundary condition

from HYCOM is not sufficient for our model to properly set up the Nova Scotian Current, as it is challenging to capture the large-scale effects from the remote wind fields over Newfoundland (Bobanović and Thompson, 2001). This remote connection between Gulf of St. Lawrence and Gulf of Maine illustrates the important impact of large-scale current systems on the non-tidal elevation and justifies the need for continental scale modeling. In limited domain modeling, this remote connection is often obscured by tweaking boundary conditions and other model parameters.

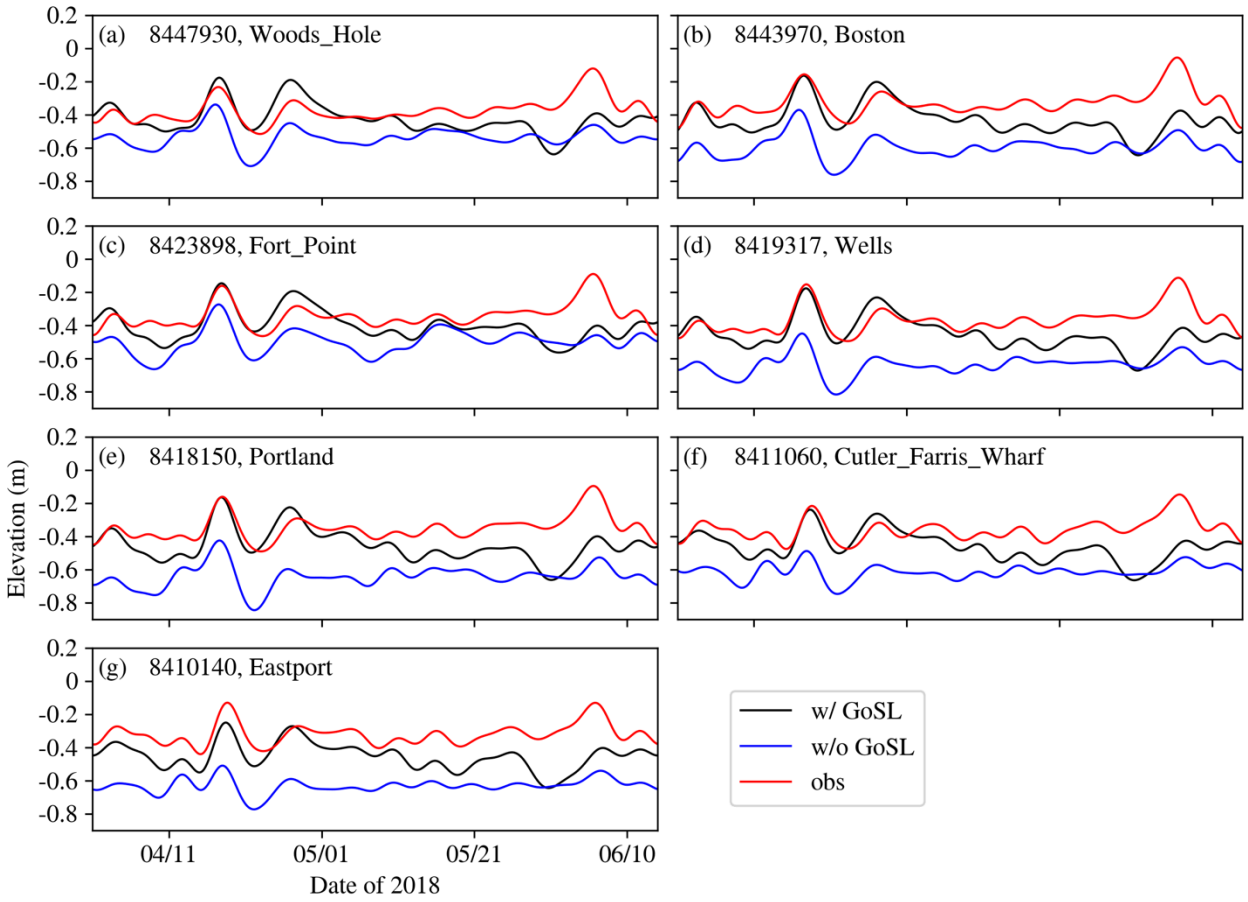

Fig. 17: Time series of low pass filtered elevation for stations in Gulf of Maine. Both observation and modeled results are referred to xGEOID20b

5. Conclusions

We have significantly improved total water level prediction at continental scale, including both near- and off-shore, using a three-pronged approach of a geoid-based datum (xGEOID20b), a satellite altimetry product (ADT) to drive the model, and a state-of-the-art 3D unstructured-grid baroclinic model. The model accurately simulated both tidal and non-tidal elevation, with an averaged RMSE of 14 cm at all NOAA stations along US east coast and Gulf of Mexico. The non-tidal signals were particularly challenging and were sensitive to the representation of large-scale current systems. The model presented in this paper has been operationalized at NOAA as the upgraded STOFS-3D-Atlantic forecast and forecast guidance results so far confirmed the findings presented in this paper.

Acknowledgements

This study was funded by NOAA [grant NA23NOS4730239]. Simulations used in this paper were conducted using the following computational facilities: (1) William & Mary Research Computing (URL: https://www.wm.edu/it/rc); (2) Texas Advanced Computing Center (TACC), The University of Texas at Austin.

References

Andres, M., 2021. Spatial and Temporal Variability of the Gulf Stream Near Cape Hatteras. J. Geophys. Res. Oceans 126, e2021JC017579. https://doi.org/10.1029/2021JC017579

Bobanović, J., Thompson, K.R., 2001. The influence of local and remote winds on the synoptic sea level variability in the Gulf of Saint Lawrence. Cont. Shelf Res. 21, 129–144. https://doi.org/10.1016/S0278-4343(00)00079-0

Ezer, T., 2018. On the interaction between a hurricane, the Gulf stream and coastal sea level. Ocean Dyn. 68 (10), 1259–1272.

Feng, Z., Li, C., 2010. Cold-front-induced flushing of the Louisiana Bays. J. Mar. Syst. 82, 252–264. https://doi.org/10.1016/j.jmarsys.2010.05.015

Frederikse, T., Simon, K., Katsman, C.A., Riva, R., 2017. The sea‐level budget along the Northwest Atlantic coast: GIA, mass changes, and large‐scale ocean dynamics. J. Geophys. Res. Oceans 122, 5486–5501. https://doi.org/10.1002/2017JC012699

GHRSST Project Office, Beggs, H., Karagali, I., Castro, S., 2023. Sea surface temperature: An introduction to users on the set of GHRSST formatted products. https://doi.org/10.5281/ZENODO.7589540

Huang, W., Ye, F., Zhang, Y.J., Park, K., Du, J., Moghimi, S., Myers, E., Pe'eri, S., Calzada, J.R., Yu, H.C., Nunez, K., Liu, Z., 2021. Compounding factors for extreme flooding around Galveston Bay during Hurricane Harvey. Ocean Model. 158, 101735. https://doi.org/10.1016/j.ocemod.2020.101735

Huang, W., Zhang, Y., Wang, Z., Ye, F., Moghimi, S., Myers, E., Yu, H. 2022. Tidal simulation revisited, Ocean Dynamics, 72:187-205. https://doi.org/10.1007/s10236-022-01498-9

Jahanmard, V., Delpeche-Ellmann, N., Ellmann, A., 2021. Realistic dynamic topography through coupling geoid and hydrodynamic models of the Baltic Sea. Cont. Shelf Res. 222, 104421. https://doi.org/10.1016/j.csr.2021.104421

Kvas, A., Brockmann, J.M., Krauss, S., Schubert, T., Gruber, T., Meyer, U., Mayer-Gürr, T., Schuh, W., Jäggi, A., and Pail, R. (2021) GOCO06s – a Satellite-Only Global Gravity Field Model. Earth System Science Data 13, no 1 (27 janvier 2021): 99118. https://doi.org/10.5194/essd-13-99-2021.

López, A.G., Wilkin, J.L., Levin, J.C., 2020. Doppio – a ROMS (v3.6)-based circulation model for the Mid-Atlantic Bight and Gulf of Maine: configuration and comparison to integrated coastal observing network observations. Geosci. Model Dev. 13, 3709–3729. https://doi.org/10.5194/gmd-13-3709-2020

Pugh, D. T. (1996). Tides, Surges and Mean Sea-Level. John Wiley & Sons Ltd.

Sheng, J., Thompson, K.R., Cong, L., Smith, P.C., Lawrence, D.J., 2001. Effect of wind and local density on the subtidal circulation of the inner Scotian Shelf. Cont. Shelf Res. 21, 1–19. https://doi.org/10.1016/S0278-4343(00)00075-3

Stephens, T.A., Savant, G., Sanborn, S.C., Wallen, C.M., Roy, S., 2022. Monolithic Multiphysics Simulation of Compound Flooding. J. Hydraul. Eng. 148, 05022003. https://doi.org/10.1061/(ASCE)HY.1943-7900.0002000

Stockdon, H.F., Long, J.W., Palmsten, M.L., Van Der Westhuysen, A., Doran, K.S., Snell, R.J., 2023. Operational forecasts of wave-driven water levels and coastal hazards for US Gulf and Atlantic coasts. Commun. Earth Environ. 4, 169. https://doi.org/10.1038/s43247-023-00817-2

Storto, A., Bonaduce, A., Feng, X., Yang, C., 2019. Steric Sea Level Changes from Ocean Reanalyses at Global and Regional Scales. Water 11, 1987. https://doi.org/10.3390/w11101987

Umlauf, L., Burchard, H., 2003. A generic length-scale equation for geophysical turbulence models. J. Mar. Res. 61, 235–265. https://doi.org/10.1357/002224003322005087

Wang, X., Chao, Y., Shum, C.K., Yi, Y., Fok, H.S., 2012. Comparison of Two Methods to Assess Ocean Tide Models. J. Atmospheric Ocean. Technol. 29, 1159–1167. https://doi.org/10.1175/JTECH-D-11-00166.1

Wang, Y., Li, X., et al. (2022) Technical Details of the Experimental GEOID 2020, NOAA Technical Report NOS NGS 78. https://geodesy.noaa.gov/library/pdfs/NOAA_TR_NOS_NGS_0078.pdf

Wang, Z., Li, D., Xue, H., Thomas, A.C., Zhang, Y.J., Chai, F., 2022b. Freshwater Transport in the Scotian Shelf and Its Impacts on the Gulf of Maine Salinity. J. Geophys. Res. Oceans 127, e2021JC017663. https://doi.org/10.1029/2021JC017663

Ye, F., Zhang, Y.J., He, R., Wang, Z., Wang, H.V., Du, J., 2019. Third-order WENO transport scheme for simulating the baroclinic eddying ocean on an unstructured grid. Ocean Model. 143, 101466. https://doi.org/10.1016/j.ocemod.2019.101466

Ye, F., Zhang, Y.J., Yu, H., Sun, W., Moghimi, S., Myers, E.P., Nunez, K., Zhang, R., Wang, H.V., Roland, A., Martins, K., Bertin, X., Du, J., and Liu, Z. 2020. Simulating storm surge and compound flooding events with a creek-to-ocean model: importance of baroclinic effects, Ocean Modelling, 145. https://doi.org/10.1016/j.ocemod.2019.101526

Ye, F., Huang, W., Zhang, Y.J., Moghimi, S., Myers, E., Pe'eri, S., Yu, H.-C., 2021. A cross-scale study for compound flooding processes during Hurricane Florence. Nat. Hazards Earth Syst. Sci. 21, 1703–1719. https://doi.org/10.5194/nhess-21-1703-2021

Ye, F., Cui, L., Zhang, Y., Wang, Z., Moghimi, S., Myers, E., Seroka, G., Zundel, A., Mani, S., Kelley, J.G.W., 2023. A parallel Python-based tool for meshing watershed rivers at

continental scale. Environ. Model. Softw. 166, 105731. https://doi.org/10.1016/j.envsoft.2023.105731

Zeng, X., Zhao, M., Dickinson, R.E., 1998. Intercomparison of Bulk Aerodynamic Algorithms for the Computation of Sea Surface Fluxes Using TOGA COARE and TAO Data. J. Clim. 11, 2628–2644. https://doi.org/10.1175/1520-0442(1998)011<2628:IOBAAF>2.0.CO;2

Zhang, Y.J., Ateljevich, E., Yu, H.-C., Wu, C.H., Yu, J.C.S., 2015. A new vertical coordinate system for a 3D unstructured-grid model. Ocean Model. 85, 16–31. https://doi.org/10.1016/j.ocemod.2014.10.003

Zhang, Y.J., Ye, F., Stanev, E.V., Grashorn, S., 2016. Seamless cross-scale modeling with SCHISM. Ocean Model. 102, 64–81. https://doi.org/10.1016/j.ocemod.2016.05.002

Zhang, Y., Ye, F., Yu, H., Sun, W., Moghimi, S., Myers, E.P., Nunez, K., Zhang, R., Wang, H.V., Roland, A., Du, J., and Liu, Z. (2020) Simulating compound flooding events in a hurricane, Ocean Dynamics, (https://doi.org/10.1007/s10236-020-01351-x)

Zhang, Y. J., Fernandez-Montblanc, T., Pringle, W., Yu, H.-C., Cui, L., and Moghimi, S., 2023. Global seamless tidal simulation using a 3D unstructured-grid model (SCHISM v5.10.0), Geoscientific Model Development, 16, 2565-2581. https://doi.org/10.5194/gmd-16-2565-2023

Zhang et al. (2024) Debunking the myths in coastal modeling, submitted to Ocean Modelling.

Zilkoski, D. B., J.H. Richards, and G.M. Young, 1992: “Results of the General Adjustment of the North American Vertical Datum of 1988.” Surveying and Land Information Systems, 52(3), 133– 149, http://www.ngs.noaa.gov/PUBS_LIB/NAVD88/navd88report.htm.